Reviews in Economic Geology, v. 20, pp. 335–363

Chapter 10

Comparison of the Allchar Au-As-Sb-Tl Deposit, Republic of Macedonia, with Carlin-Type Gold Deposits

Sabina Strmić Palinkaš,[1,†] Albert H. Hofstra,[2] Timothy J. Percival,[3] Sibila Borojević Šoštarić,[4] Ladislav Palinkaš,[5] Vladimir Bermanec,[5] Zoltan Pecskay,[6] and Blazo Boev[7]

[1] *UiT The Arctic University of Norway, Faculty of Science and Technology, Department of Geosciences, Dramsvegen 201, N-9037 Tromsø, Norway*

[2] *U.S. Geological Survey, Denver Inclusion Analysis Laboratory (DIAL), P.O. Box 25046, MS 963, Denver, Colorado 80225, USA*

[3] *Consulting Economic Geologist, 3240 Quartzite Drive, Reno, Nevada 89523, USA*

[4] *University of Zagreb, Faculty of Mining, Geology, and Petroleum Engineering, Pierottijeva 6, HR-10000 Zagreb, Croatia*

[5] *University of Zagreb, Faculty of Science, Geological Department, Horvatovac 95, HR-10000 Zagreb, Croatia*

[6] *Institute of Nuclear Research, Hungarian Academy of Sciences, Bem tér 18/C, H-4001 Debrecen, Hungary*

[7] *Goce Delčev University, Faculty of Natural and Technical Sciences, Goce Delčev 89, MK-2000 Štip, Republic of Macedonia*

Abstract

The Allchar Au-As-Sb-Tl deposit is situated in the western part of the Vardar zone, the main suture zone along the contact between the Adriatic and the Eurasian tectonic plates. It is spatially and temporally associated with a Pliocene (~5 Ma) postcollisional high-K calc-alkaline to shoshonitic volcano-plutonic center.

The Allchar deposit shares many distinctive features with Carlin-type gold deposits in Nevada, including its location near a terrain-bounding fault in an area of low-magnitude extension and intense magmatism. The mineralization is mostly hosted in calcareous sedimentary rocks at intersections of high-angle faults in permeable stratigraphy. The alteration types (carbonate dissolution, silicification, and argillization), ore mineralogy (auriferous arsenian pyrite and marcasite, stibnite, realgar, orpiment, and lorandite), high Au/Ag ratios, and low base metal contents are also typical of Carlin-type gold deposits in Nevada.

However, the Allchar deposit differs from Nevada Carlin-type gold deposits as follows: it is an isolated Au prospect with a close spatial and temporal relationship to a shoshonitic volcano-plutonic center in a mineral belt dominated by intrusion-related Cu-Au porphyry, skarn, and hydrothermal polymetallic deposits. The deposit is clearly zoned (proximal Au-Sb to distal As-Tl), it has a significantly higher Tl content, trace elements in pyrite and marcasite are homogeneously distributed, and synore dolomitization is a widespread alteration type.

Gold mineralization is most abundant in the southern part of the deposit. It occurs mostly as invisible Au in disseminated pyrite or marcasite and as rare native Au grains. Gold mineralization is accompanied by intense decarbonatization and silicification. Fluid inclusions and the hydrothermal alteration mineral assemblage indicate that Au was deposited from hot (>200°C), saline (up to ~21 wt % NaCl equiv), moderately acidic (pH <5) fluids that carried traces of magmatic H_2S and CO_2. In the calcareous host rocks, mixing of such fluids with cool, dilute, near-neutral groundwater triggered deposition of Au and Fe sulfides. In Tertiary tuff, isocon analysis shows that sulfidation of preexisting Fe minerals was a critical factor for deposition of Au and Fe sulfides.

Antimony mineralization prevails in the central part of the deposit, and it is mostly associated with dark-gray to black jasperoid. Stibnite, the most common Sb mineral in the Allchar deposit, occurs as fine-grained disseminations in jasperoid and as fine- to coarsely crystalline masses that fill vugs and fracture zones lined with drusy quartz. Fluid inclusions entrapped by stibnite-bearing jasperoid, quartz, and calcite crystals suggest that stibnite was deposited from more dilute and cooled fluids (aqueous-carbonic fluid inclusions: 6.0–3.5 wt % NaCl equiv, T_H = 102°–125°C; aqueous fluid inclusions: 14.5 and 17.1 wt % NaCl equiv, T_H = 120°–165°C).

In contrast to stibnite, As sulfides (orpiment and realgar) and Tl mineralization are associated with argillic alteration. Fluid inclusions hosted by realgar, orpiment, dolomite, and lorandite record deposition from more dilute (2.6–6.9 wt % NaCl equiv) and relatively cold fluids (T_H = 120°–152°C) enriched in K. Isocon diagrams show a tight link between Tl and the low-temperature argillic alteration as well as a significant correlation between Tl and K. The spatial relationship of Tl mineralization with dolomite suggests that Tl deposition was also promoted by neutralization of acidic fluids.

The δD and $\delta^{18}O$ data obtained from gangue minerals and fluid inclusions indicate that magmatic fluid mixed with exchanged meteoric water at deep levels and with unexchanged meteoric water at shallow levels in the system. The $\delta^{13}C$ and $\delta^{18}O$ values of carbonate minerals and extracted fluid inclusions suggest mixing of carbonate rock buffered fluids with magmatic and atmospheric CO_2. The sulfur isotope values of early disseminated pyrite and marcasite show that H_2S was initially derived from diagenetic pyrite in sedimentary rocks. In contrast, Sb and As mineralization indicate a strong input of magmatic H_2S during the main mineralization stage. Late-stage botryoidal pyrite and marcasite are depleted in ^{34}S, which indicates a diminishing magmatic influence and predominance of sulfur from sedimentary sources during the late-mineralization stage. Fractionation of isotopically light sulfide species from isotopically heavy sulfates due to oxidation under increased oxygen fugacity cannot be excluded.

[†]Corresponding author: e-mail, sabina.s.palinkas@uit.no

doi: 10.5382/rev.20.10; 29 p.
Supplementary files available online at www.segweb.org/REV20-Appendices.

Introduction

The Allchar Au-As-Sb-Tl deposit (also spelled Alshar and Alšar) is situated on the northwestern slopes of the Kožuf Mountains approximately 110 km southeast from Skopje, Republic of Macedonia (Fig. 1). Mining activities began ~800 to 300 B.C. with the Ancient Greeks. In the 19th century, Allchar was an important source of As for the Ottoman Empire and in the mid-20th century it reopened as an Sb mine. Due to the elevated As content in the Sb concentrate, production ceased after fewer than 10 years. In 1980s and 1990s, the area was prospected for Tl and Au. In 1990, Percival reported a large Au anomaly in the central and southern portions of the deposit. Allchar is estimated to contain approximately 500 t of Tl, making it one of the largest Tl anomalies in the world (Janković and Jelenković, 1994; Percival and Radtke, 1994; Bačeva et al., 2014).

The deposit has distinctive features of Carlin-type gold deposits in Nevada such as (1) strong structural control of mineralization by faults and folds; (2) temporal and spatial association with magmatism in an extensional setting; (3) calcareous sedimentary host rocks; (4) alteration types including decarbonatization, silicification, argillization, and sulfidation; (5) submicron gold in association with pyrite and marcasite; and (6) geochemical signatures of Au, As, Hg, Sb, and Tl (Radtke, 1985; Hofstra and Cline, 2000; Muntean et al., 2011). However, it differs from Nevada Carlin-type gold deposits in several ways, including the following: (1) it is significantly smaller in size; (2) some of the mineralization is hosted in Tertiary tuff; (3) mineralization is spatially associated with shoshonitic magmatism; (4) there is a zonal distribution of metals in the deposit; (5) it includes homogeneous distribution of trace elements in Au-bearing pyrite and marcasite; (6) dolomitization is a widespread alteration type, especially in the northern part of the deposit; and (7) it has high Tl content.

This paper summarizes new and previously published data on the geotectonic evolution of the region, age constraints provided by alteration and mineralization in volcanic rocks, lithogeochemical characteristics of country rocks and mineralization, chemical composition of Fe-, Sb-, As-, and Tl sulfides, microthermometry of fluid inclusions, and stable isotopic compositions of ore and gangue minerals and entrapped fluid inclusions. These data are used to place Allchar into the metallogenic evolution of the region, determine the chemistry and origin of hydrothermal fluids and processes of mineralization, and facilitate comparison to Carlin-type gold deposits in Nevada.

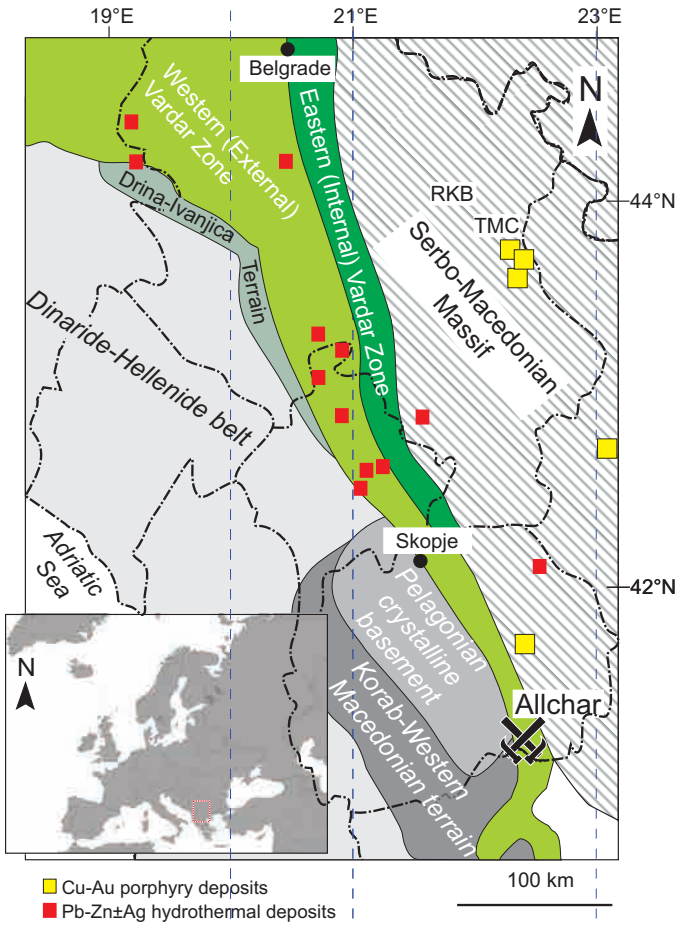

Fig. 1. Regional geologic setting of the Allchar Au-As-Sb-Tl deposit, Republic of Macedonia, within the Balkan Peninsula (simplified after Dimitrijević, 2001, and Karamata, 2006). The locations of the most prominent Pb-Zn ± Ag hydrothermal and Cu-Au porphyry deposits are also marked. Abbreviations: RKB = Ridanj-Krepoljin belt, TMC = Timok magmatic complex.

Geologic Setting

Regional geology

The Allchar Au-As-Sb-Tl deposit is situated in the western part of the Vardar zone, in close proximity to its contact with the Pelagonian crystalline basement (Fig. 1). The Vardar zone represents the main suture zone along the contact between the Adriatic and the Eurasian plate with elements of both continental and oceanic rock types (Karamata et al., 2000; Dimitrijević, 2001; Zelić et al., 2010; Robertson et al., 2013). It extends from northwest to southeast across the central part of the Balkan Peninsula and is situated between the Dinarides, Drina-Ivanjica terrain, Korab-Western Macedonian terrain, and Pelagonian crystalline basement on the west and the Serbo-Macedonian massif on the east (Fig. 1).

During the Late Permian to Middle Triassic, incipient rifting affected metamorphosed Precambrian-Paleozoic terrains between the Pelagonian crystalline basement and the Serbo-Macedonian massif. Rifting was followed by the development of a subsiding carbonate platform and formation of oceanic crust during Late Triassic-Early Jurassic time (Sharp and Robertson, 2006; Dilek et al., 2007; Robertson et al., 2013). The western (external) Vardar zone represents a complex zone that comprises ophiolites and ophiolitic mélange (Karamata et al., 1980). At several localities the ophiolitic masses, composed of spinel lherzolite, harzburgite, and dunite, preserve evidence of metamorphic soles at their base. The K/Ar age between 160 and 123 Ma (Karamata et al., 2000) and Ar/Ar age between 175 and 170 Ma (Borojević Šoštarić et al., 2014) obtained from the metamorphic soles suggest emplacement of the ophiolites from Middle Jurassic to Early Cretaceous. The Jurassic-Cretaceous mélange of the western Vardar zone is composed of large blocks and fragments of Middle to Upper Triassic and Upper Jurassic limestones, terrigenous sediments (sandstone, graywacke), basalts, and cherts with Carnian to

Norian and Upper Jurassic radiolarians within an argillaceous to silty matrix (Sudar and Kovacs, 2006; Vasković and Matović, 2010). In contrast, the eastern (internal) Vardar zone consists of weakly metamorphosed mélange of Jurassic age with predominantly basaltic fragments (Sudar and Kovacs, 2006, and references therein).

On the Balkan Peninsula, subduction-related igneous rocks of Upper Cretaceous age are exposed in the Timok Magmatic Complex and Ridanj-Krepoljin belt in eastern Serbia (Fig. 1; Janković, 1997; Karamata et al., 1997; von Quadt et al., 2005; Zimmerman et al., 2008). From the beginning of the Tertiary, the central Balkan Peninsula was affected by collisional to transpressive deformation followed by several postcollisional episodes of extension (Cvetković et al., 2004).

Postcollisional igneous rocks of Oligocene-Pliocene age (29.0–1.8 Ma) occur at numerous localities along the Vardar zone in Serbia, Kosovo, Macedonia, and Greece (e.g., Kolios et al., 1980; Janković et al., 1997, Cvetković et al., 2004; Yanev et al., 2008, Lehmann et al., 2013). Magmatism occurred in an extensional tectonic setting and was accompanied by widespread hydrothermal activity that produced numerous porphyry, skarn, hydrothermal polymetallic replacement, and vein deposits (Fig. 1; Janković, 1995; Veselinović-Williams, 2011; Borojević Šoštarić et al., 2013; Lehmann et al., 2013; Strmić Palinkaš et al., 2013).

Geology of the Kožuf massif

The Kožuf massif (Voras massif in Greece; Fig. 2) is situated on the border between the Republic of Macedonia and Greece. In the east, it occurs in fault contact with the Demir Kapija-Gevgelija ophiolite complex (Fig. 2). In the west, it is in fault contact with the Pelagonian massif (Fig. 1). The Kožuf massif basement is at least partly composed of Precambrian gneisses and marbles (Fig. 2) that are conformably overlain by Paleozoic metasedimentary rocks—mostly phyllites, schists, metasandstones, and marbles. The Mesozoic metasedimentary complex comprises Triassic marbles, dolostones, and shales; Jurassic schists, quartzites, and cherts; and Cretaceous limestones and conglomerates. Upper Eocene basal conglomerates are overlain by flysch sediments, late Miocene to Pleistocene shoshonitic volcanic rocks (Yanev et al., 2008), and Pliocene lacustrine sediments (Rakičević and Pendžerkovski, 1970; Mercier, 1973; Boev, 1988).

Geology of the Allchar Au-As-Sb-Tl deposit

The Allchar Au-As-Sb-Tl deposit is hosted by the Mesozoic metasedimentary complex and unconformable Tertiary volcanic and carbonate rocks (Fig. 3; Ivanov, 1965; Percival and Radtke, 1994). The southwestern flank of the district is bordered by tectonically emplaced Jurassic ophiolites and ophiolitic mélange (Fig. 2). The Mesozoic metasedimentary complex comprises Triassic marble, dolomite, and schists that are products of regional greenschist facies metamorphism. Marble is the most abundant pre-Tertiary rock in the district and consists of gray-white to bluish-gray, fine- to medium-grained equigranular calcite intercalated with minor detrital material. The dolomite is gray-white to tan, fine to medium grained, and locally recrystallized to dolomitic marble. The schists vary in their composition from quartz-sericite and chloritic schists to graphitic schists. They are well exposed in the eastern part of the deposit (Percival and Radtke, 1994).

Tertiary dolomite is usually massive to fine grained, and it lies above the Eocene unconformity on Mesozoic metasedimentary rocks (Fig. 3; Percival and Radtke, 1994). The

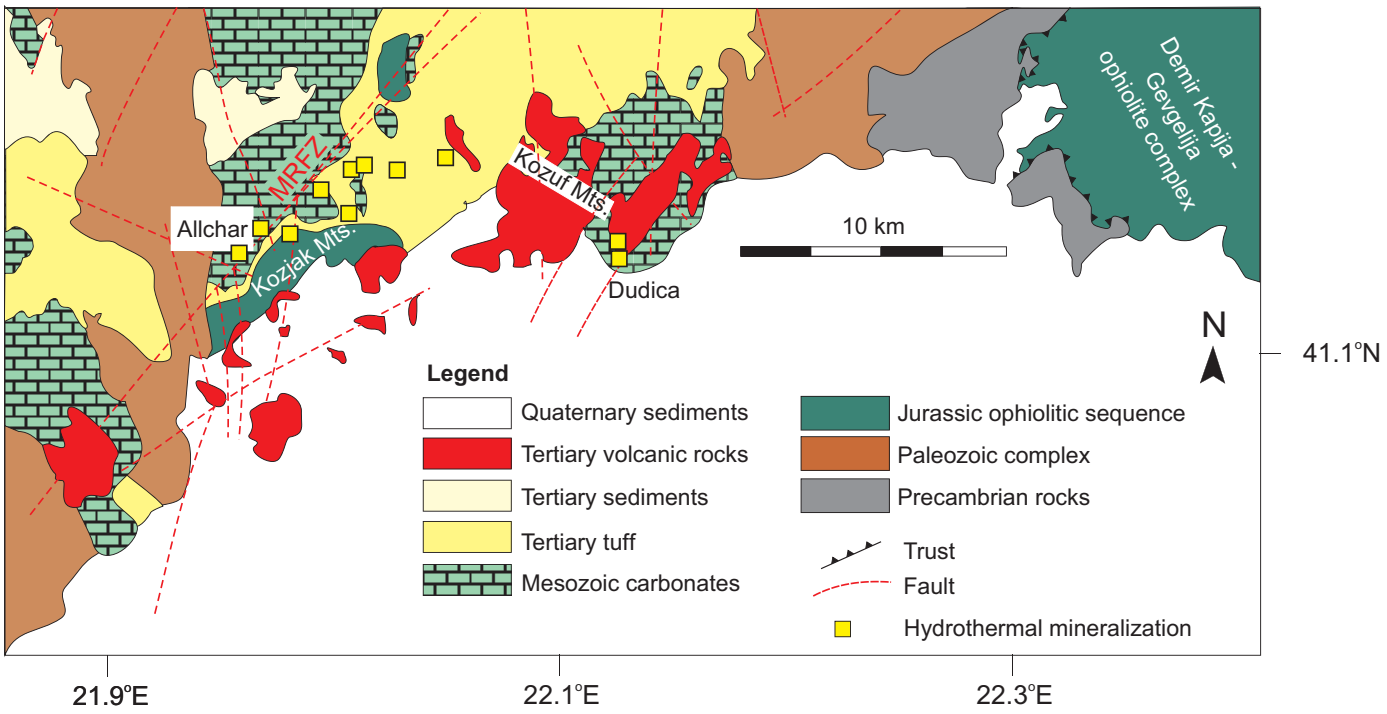

Fig. 2. Geologic map of the Kožuf massif (simplified after Boev, 1988, and Božović et al., 2013). Abbreviations: MRFZ = Majdan River fault zone.

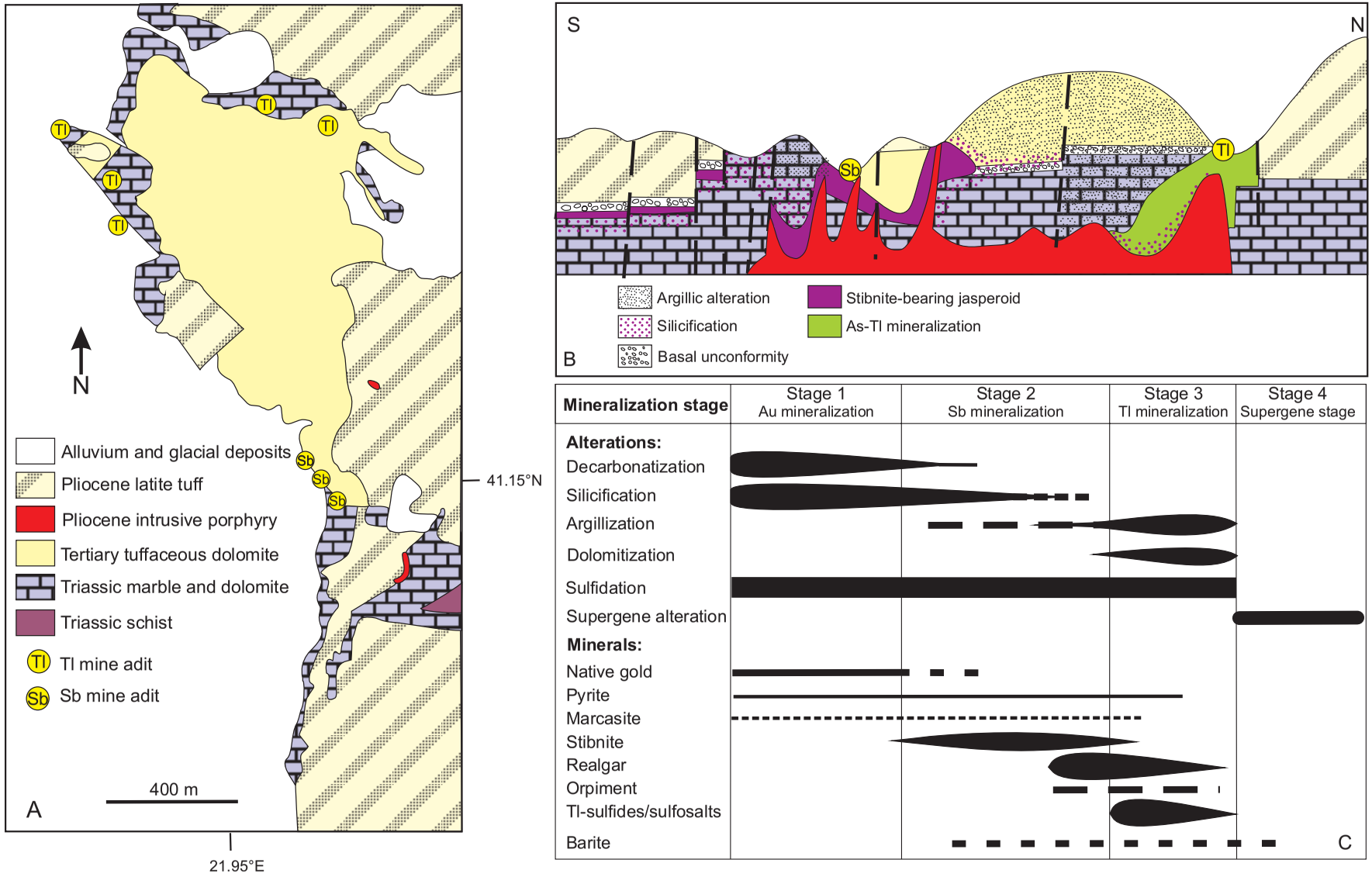

Fig. 3. (A) Geologic map of the Allchar Au-As-Sb-Tl district, Republic of Macedonia. (B) North-south longitudinal section through the Allchar district showing geologic, alteration, and mineralization relationships among the northern, central, and southern portions of the district (after Percival and Radtke, 1994). (C) The paragenetic sequence of the Allchar Au-As-Sb-Tl.

unconformity is a zone with silt- to cobble-sized rocks of mixed characteristics. This porous and permeable zone is often altered and variably mineralized. The dolomite was deposited in a lacustrine basin and contains dispersed and intercalated tuffaceous debris. Numerous lacustrine basins were formed as a result of Miocene extensional tectonism in other areas underlain by carbonate and ultramafic rocks along the Vardar zone (Ilić Jr., 1988; Dumurdzanov et al., 2004; Jurković et al., 2012). Pliocene tuffaceous volcanic and volcaniclastic rocks overlie Tertiary dolomite and Mesozoic metasedimentary rocks (Fig. 3; Percival and Radtke, 1994).

Hypabyssal intrusions cut the Mesozoic and Tertiary rocks, except the Pliocene tuffaceous units that are probably contemporaneous with the intrusions. The intrusions are typically porphyritic and intensely altered. They range in composition from latite to andesite and commonly contain significant amounts of sulfides. Similar hydrothermally altered intrusions occur in the underground antimony and arsenic-thallium mines (Fig. 3; Percival and Radtke, 1994).

N-, NW-, and NE-trending, steeply dipping fault sets in the Allchar deposit (Fig. 2) are characterized by sheared, brecciated, and fractured wall rocks, stratigraphic juxtaposition, and topographic discontinuities and are commonly the locus of intense hydrothermal alteration and variable sulfide deposition. The Majdan River fault zone and associated N-trending structures (Fig. 2) located to the west of the antimony mines are defined by a major topographic discontinuity between pervasively altered and mineralized cliff-like outcrops of carbonate rocks to the east and glacial till-covered, low-relief, rolling hills to the west. This structure is believed to have originated from north-south strike-slip movement along the Vardar zone. The NW- and NE-trending structures formed as dilational conjugate sets of faults in response to the north-south shearing. These faults are the most intensely brecciated and crackled carbonate rocks in the district and provided permeability and open spaces that facilitated movement of hydrothermal fluids.

Hydrothermal alteration

In the Allchar deposit, hydrothermal alteration is widespread and has a zonal distribution relative to the mineralization (Fig. 3). The principal alteration types include (1) carbonate dissolution (decarbonatization), (2) silicification, (3) argillization, (4) dolomitization, (5) sulfidation, and (6) supergene alteration of sulfide minerals (Janković, 1993; Percival and Radtke, 1993a, 1994).

Carbonate dissolution (decarbonatization) represents the earliest type of hypogene alteration. It affected Triassic and Tertiary carbonate rock types, resulting in the removal of calcite and dolomite with resultant increases in porosity and permeability. Decarbonatization is typically accompanied by silicification and argillization, and it exhibits a lateral transition from fresh to bleached, partially altered, and completely altered rocks. In places, Tertiary dolomite was decarbonatized without accompanying silicification. Decarbonatization resulted in dissolution of the fine-grained carbonate matrix, leaving predominantly granular dolomite sand, iron oxides, jarosite, and greenish to yellowish unidentified secondary minerals. Similar textures have been described in other Carlin-type deposits hosted in dolomite (e.g., Hofstra and Cline, 2000; Cline et al., 2003, 2005).

Pervasive silicification occurs in both pre-Tertiary and Tertiary rocks, and its intensity varies from weak to total replacement (jasperoid). Jasperoidal silicification is typically composed of dark-gray to black, fine-grained, dense, microcrystalline quartz exhibiting xenomorphic and jigsaw textures that thoroughly obliterate original textures. Less silicified rocks contain varying proportions of argillic clays and sericite mixed with microcrystalline quartz that are crosscut by quartz veinlets containing disseminated pyrite, marcasite, and rare crystalline masses of stibnite, realgar, and barite. This type of silicification is most prevalent in the tuffaceous volcanic rocks and volcaniclastic horizons in the Tertiary carbonate sequence.

Argillic and sericitic alterations are voluminous and occur in volcanic and sedimentary rocks. Alteration is pervasive adjacent to faults and silicified zones and is strong in the Tertiary tuffs and tuffaceous dolomites. Argillic assemblages typically envelope silicified zones decreasing in intensity with increasing distance from silicification (Fig. 3). X-ray diffraction studies of the clay-altered rocks indicate that they contain varying proportions of the following minerals: kaolinite, sericite, illite-group minerals (including celadonite), hydromicas, pyrophyllite, and subordinate chlorite (Percival and Radtke, 1994).

Dolomitization of Triassic marble is spatially associated with mineralization (Fig. 3). Dolomitized rocks are typically lighter colored than the host marble and transitionally grade into undolomitized marble (Percival and Radtke, 1994).

Supergene alteration is widespread and typical of humid environments. Pyrite and marcasite are replaced by Fe oxides and hydroxides; As, Sb, and Tl sulfides form oxides; and igneous and sedimentary rocks are converted to mixtures of secondary clay minerals.

Mineralization

Mineralization in the Allchar deposit is zoned (Fig. 3). The southern part of the deposit is characterized by significant amounts of siliceous Au mineralization. The Au content decreases northward. In the central part of the deposit, Sb-bearing jasperoid prevails. The northernmost part of the deposit is characterized by As- and Tl-bearing minerals in strongly altered rocks.

Gold mineralization is hosted in weakly to moderately silicified Tertiary tuffs and Triassic marbles (Fig. 4A). Silicified ore contains finely disseminated pyrite with minor amounts of stibnite, marcasite, and realgar. Gold occurs as submicron invisible Au in disseminated pyrite or marcasite (Fig. 4B) or as rare native micron-sized grains (Fig. 4C). Gold grades are variable and commonly vary from 0.5 to 10 g/t Au (Percival and Radtke, 1994).

Stibnite-bearing jasperoids were mined extensively for their Sb content (Janković, 1979). The jasperoids are dark-gray to black and are composed of fine-grained, mosaic-textured microcrystalline quartz (Fig. 5A). Most jasperoids are fractured and brecciated and contain veinlets and irregular masses of coarser crystalline, gray to white quartz. The microcrystalline quartz matrix contains finely disseminated sulfides (1–5%), fine-grained sericite, and silicified host-rock clasts containing sericite and sulfides. Pyrite is commonly the most abundant sulfide mineral. It occurs as fine (<0.5 mm) disseminated grains, larger (>0.5 mm) subhedral to euhedral crystals,

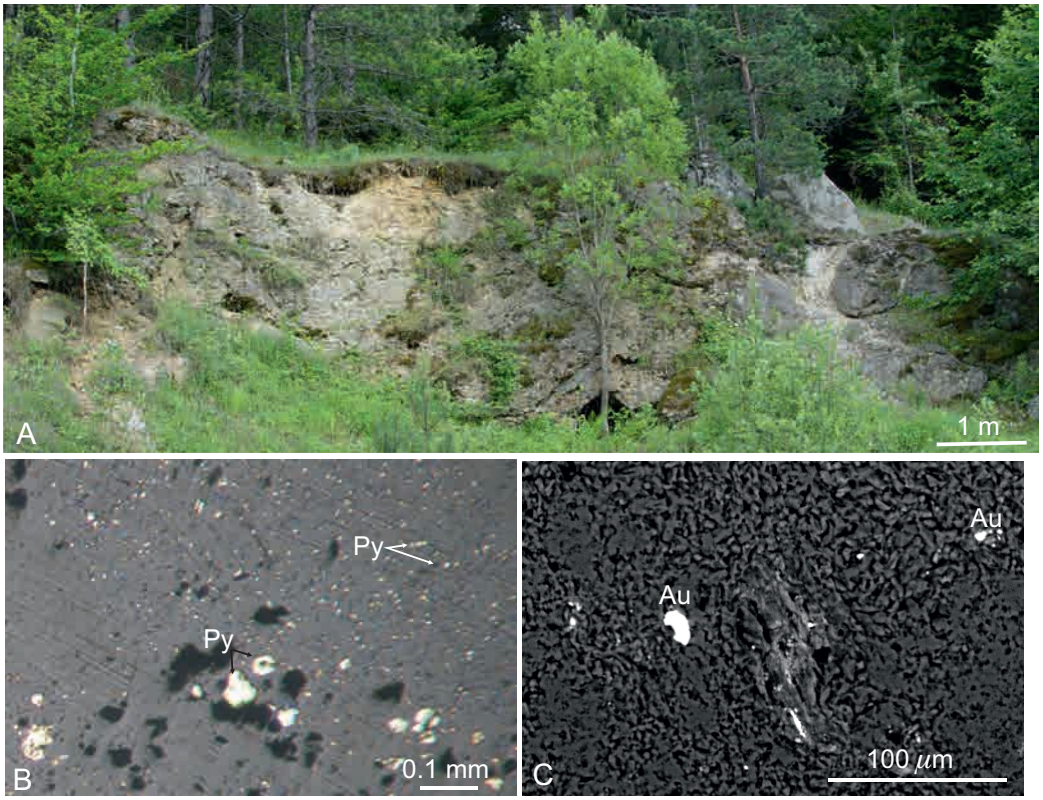

Fig. 4. (A) Silicified Tertiary tuff in the southern part of the Allchar Au-As-Sb-Tl deposit. (B) Reflected-light photomicrograph of the siliceous Au mineralization. Gold occurs as invisible Au, usually as an enrichment in disseminated pyrite or marcasite. (C) Scanning electron photomicrograph of rare individual Au grains disseminated within silicified tuff. Abbreviations: Py = pyrite.

and aggregates of coarse-grained crystals. Sparse, finely crystalline arsenopyrite, marcasite, and stibnite are also present (Fig. 5B). The later coarse sulfide stage is characterized by coarse-grained sulfide minerals occurring as linings and infillings of open spaces in breccia and fracture zones within jasperoidal silica. Marcasite and pyrite occur in banded veins and as botryoidal masses (Fig. 5C). Late stibnite occurs as fine to coarsely crystalline masses, acicular crystals filling vugs and fractures, and breccia cement (Fig. 5D). Paragenetically late realgar occurs as distinct crystals, crystallized aggregates, masses, and overgrowths on all other minerals (Fig. 5E). The stibnite-bearing jasperoids commonly contain from 1 to 3 g/t Au, and locally the Au content exceeds 20 g/t (Percival and Radtke, 1994).

The arsenic mineralization is hosted in argillized tuffs, in Tertiary dolomite, and rarely in Triassic carbonate rocks distal to the zones of jasperoidal silicification. Host rocks are pervasively altered to clays and sericite mixed with sulfides and subordinate hydrothermal silica. The sulfide minerals typically compose >10 and up to 50 vol % of the host rock (Fig. 6A). The sulfide assemblage includes disseminated marcasite and pyrite associated with abundant finely to coarsely crystallized realgar and subordinate orpiment, stibnite, and minor thallium-bearing sulfosalt minerals (Fig. 6B). The Au content is typically lower than the siliceous mineralization and usually varies from <1 to 3 g/t (Percival and Radtke, 1994).

The Tl-bearing mineralization is hosted by carbonate and tuffaceous rocks in the northern portion of the deposit (Fig. 7A). The most prominent Tl mineralization is concentrated within the Crven Dol orebody (Ivanov, 1986; Janković, 1993; Janković and Jelenković, 1994). This part of the deposit is strongly affected by argillic alteration. The mineralization is composed of mixtures of orpiment, realgar, pyrite, marcasite, lorandite ($TlAsS_2$), and rare Tl-bearing sulfosalt minerals including vrbaite ($Tl_4Hg_3Sb_2As_8S_{20}$), picopaulite ($TlFe_2S_3$), rebulite ($Tl_5Sb_5As_8S_{22}$), simonite ($TlHgAs_3S_6$), bernardite ($Tl[As,Sb]_5S_8$), raguinite ($TlFeS_2$), parapierrotite ($Tl[Sb,As]_5S_8$), jankovićite ($Tl_5Sb_9[As,Sb]_4S_{22}$), weissbergite ($TlSbS_2$), fangite (Tl_3AsS_4), dorallcharite ($Tl_{0.8}K_{0.2}Fe_3[SO_4]_2[OH]_6$), and thalliumpharmacosiderite ($TlFe_4[(AsO_4)_3(OH)_4]\cdot 4H_2O$) (Pavićević and El Goresy, 1988; Percival and Radtke, 1993b, 1994; Balić-Žunić et al., 1994; Frantz et al., 1994; Cvetković et al., 1995; Rumsey et al., 2014). Sulfide and sulfosalt minerals typically occur as disseminations and as fracture, open space, and breccia infillings (Fig. 7B). Locally, As-Tl mineral assemblages occur as massive sulfide (>5–30 vol %) replacements in the carbonate-bearing rock (Fig. 7; Percival and Radtke, 1994).

Analytical Methods

This paper presents new data on mineral chemistry, stable isotopes, and fluid inclusions from the Allchar Au-As-Sb-Tl deposit and combines them with previously published geochronological data (Table 1; Kolios et al., 1980; Jakupi et al., 1982; Lippolt and Fuhrmann, 1986; Boev, 1988; Troesh and Frantz, 1994; Neubauer et al., 2009; Strmić Palinkaš et al., 2012),

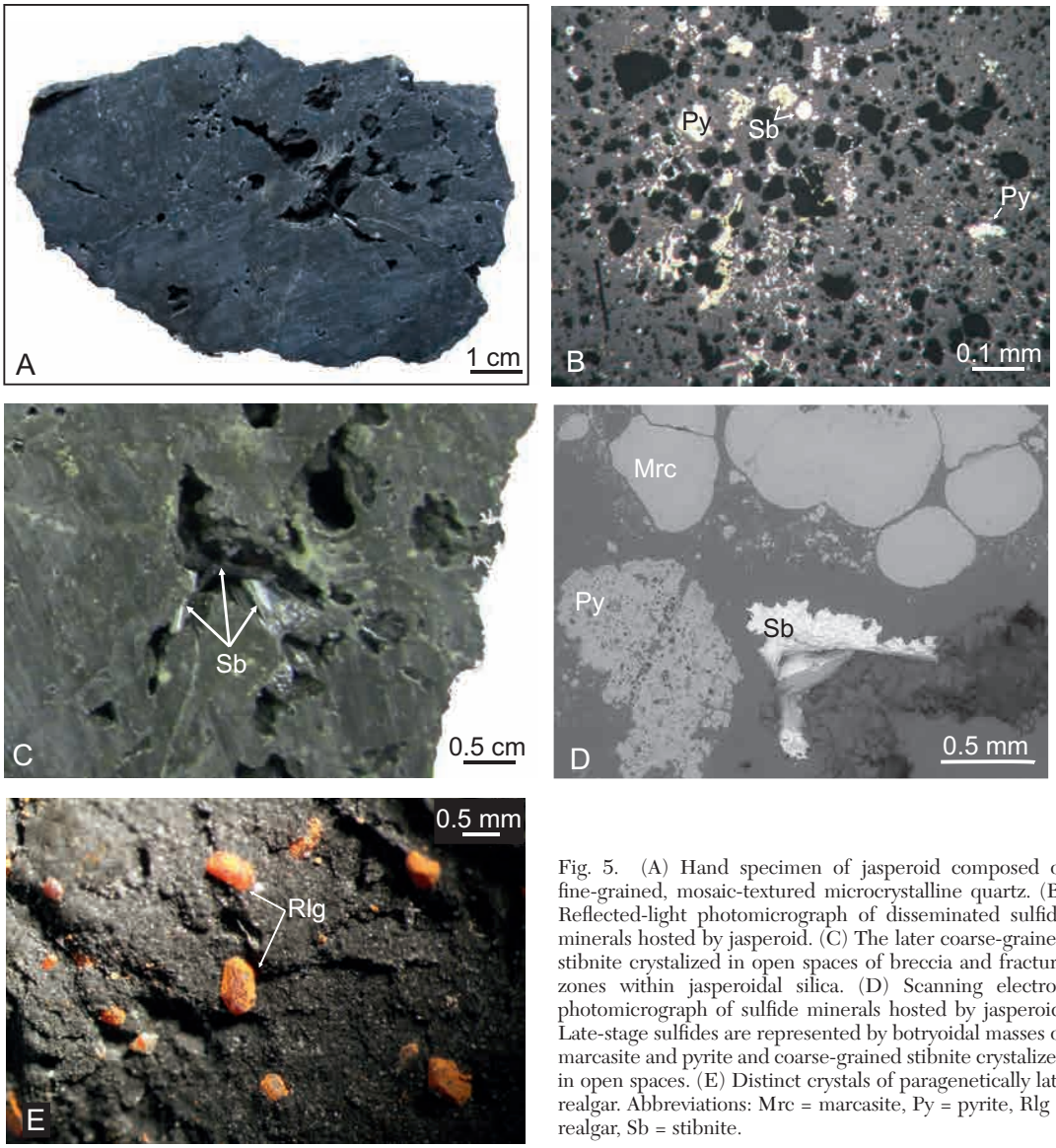

Fig. 5. (A) Hand specimen of jasperoid composed of fine-grained, mosaic-textured microcrystalline quartz. (B) Reflected-light photomicrograph of disseminated sulfide minerals hosted by jasperoid. (C) The later coarse-grained stibnite crystalized in open spaces of breccia and fracture zones within jasperoidal silica. (D) Scanning electron photomicrograph of sulfide minerals hosted by jasperoid. Late-stage sulfides are represented by botryoidal masses of marcasite and pyrite and coarse-grained stibnite crystalized in open spaces. (E) Distinct crystals of paragenetically late realgar. Abbreviations: Mrc = marcasite, Py = pyrite, Rlg = realgar, Sb = stibnite.

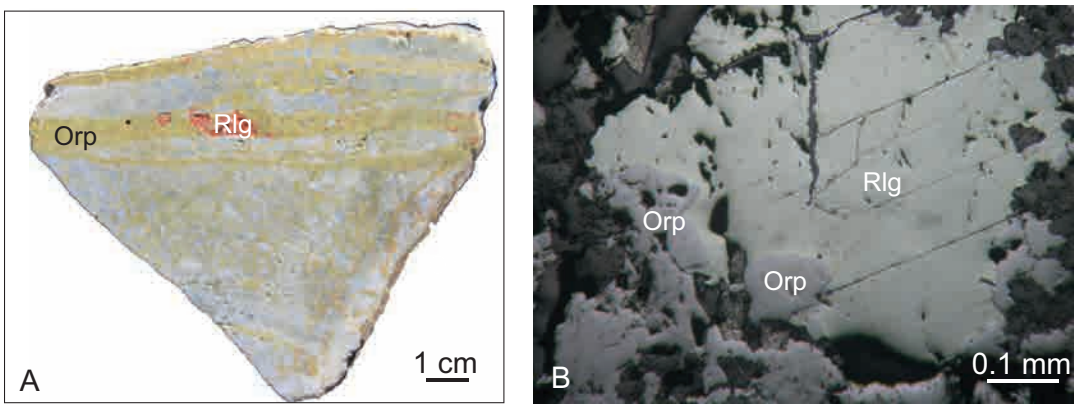

Fig. 6. (A) Arsenic mineralization hosted by argillized Tertiary tuff. (B) Reflected-light photomicrograph of arsenic mineralization. Abbreviations: Orp = orpiment, Rlg = realgar.

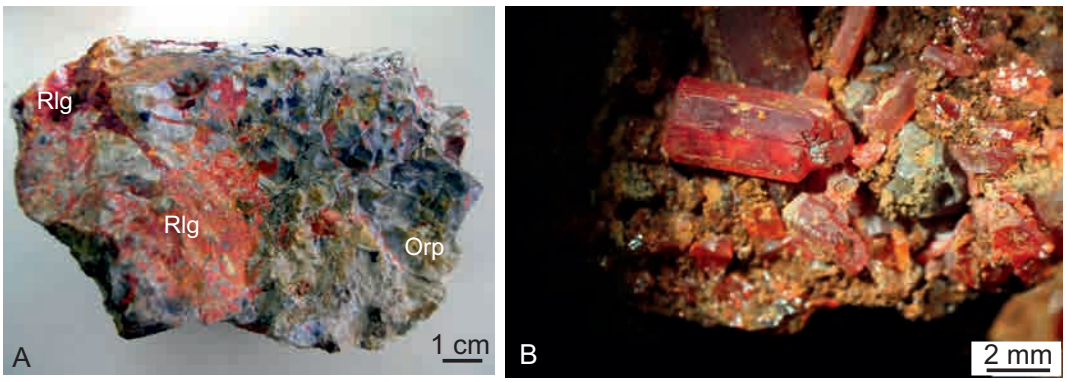

Fig. 7. (A) The Tl-bearing mineralization is hosted by brecciated Tertiary dolomite. (B) Lorandite crystals deposited along fractures of brecciated Tertiary dolomite. Abbreviations: Orp = orpiment, Rlg = realgar.

lithogeochemical data (Electronic App. 1; Percival and Radtke, 1994; Yanev et al., 2008; Boev and Jelenković, 2012), Pb isotope data (Electronic App. 2; Frantz et al., 1994), stable isotope data (Tables 2, 3; Janković, 1993; Frantz et al., 1994; Volkov et al., 2006), and fluid inclusion data (Strmić Palinkaš et al., 2012).

Microanalyses of sulfide minerals were conducted using laser ablation-inductively coupled plasma-mass spectrometry (LA-ICP-MS; Ridley and Lichte, 1998) at the U.S. Geological Survey (USGS), Denver, Colorado, to investigate the siting of Au and the distribution of major and trace elements including As, Bi, Co, Fe, Ga, Ge, Hg, In, Mn, Mo, Ni, Pb, Re, S, Sb, Se, Te, Tl, U, W, and Zn. Where Au, Ag, and Sb in sulfide minerals were near or below the detection limits of the microprobe, LA-ICP-MS was used. Fe, S, and As concentrations measured by microprobe analysis were used to standardize between methods.

Stable isotope studies of hydrogen, carbon, oxygen, and sulfur were carried out in the stable isotope laboratory at the USGS. Carbonate minerals were analyzed by reaction with 100% phosphoric acid at 25°C based on McCrea (1950). The acid fractionation factors of Friedman and O'Neil (1977) were used. Sulfur isotope analyses were carried out using a continuous flow method similar to that described by Giesemann et al. (1994). Hydrogen, carbon, and oxygen isotope analyses were also performed on fluid inclusion extracts liberated by thermal decrepitation in stainless steel tubes. Isotopic compositions of gases were measured using either a Finnigan MAT 252 or a Micromass Optima isotope ratio mass spectrometer. Isotopic compositions are reported in δ notation relative to Vienna-standard mean ocean water (V-SMOW) for oxygen and hydrogen, Pee-Dee belemnite (PDB) for carbon, and Canyon Diablo Troilite (CDT) for sulfur.

Table 1. Geochronological Data from the Allchar Au-As-Sb-Tl Deposit, Republic of Macedonia

Mineralogy	Host rock/mineralization	Locality	Age (Ma)	Method	Reference
Biotite	High-K calc-alkaline to shoshonitic volcanic rocks	Kožuf massif	1.9 ± 0.1–5.0 ± 0.2	K/Ar	Kolios et al. (1980)
K-feldspar	High-K calc-alkaline to shoshonitic volcanic rocks	Kožuf massif	1.8 ± 0.1– 4.5 ± 0.2	K/Ar	Kolios et al. (1980)
Whole rock	High-K dacitic lava	Kožuf massif	4.6 ± 0.2	K/Ar	Kolios et al. (1980)
Biotite	Latite	Kožuf massif	1.8 ± 0.1–5.0 ± 0.2	K/Ar	Boev (1988)
Biotite	Qtz latite	Kožuf massif	6.5 ± 0.2	K/Ar	Boev (1988)
Biotite	Andesite	Kožuf massif	4.8 ± 0.2	K/Ar	Boev (1988)
Whole rock	Qtz latite	Kožuf massif	4.62 ± 0.19	K/Ar	Strmić Palinkaš et al. (2012)
Amphibole	Qtz latite	Kožuf massif	5.79 ± 0.21	K/Ar	Strmić Palinkaš et al. (2012)
Biotite	Qtz latite	Kožuf massif	5.61 ± 0.20	K/Ar	Strmić Palinkaš et al. (2012)
K-feldspar	Qtz latite	Kožuf massif	5.15 ± 0.21	K/Ar	Strmić Palinkaš et al. (2012)
Orpiment	Tl mineralization	Crven dol, Allchar deposit	5	Fission track	Jakupi et al. (1982)
K-feldspar	Andesite	Crven dol, Allchar deposit	4.8 ± 1.9	K/Ar	Lippolt and Fuhrmann (1986)
Biotite	Andesite	Crven dol, Allchar deposit	5.1 ± 1.9	K/Ar	Lippolt and Fuhrmann (1986)
Whole rock	Andesite	Crven dol, Allchar deposit	3.9 ± 0.2	K/Ar	Lippolt and Fuhrmann (1986)
K-feldspar	Tuff	Crven dol, Allchar deposit	4.4 ± 0.5–4.6 ± 0.4	K/Ar	Lippolt and Fuhrmann (1986)
Biotite	Tuff	Crven dol, Allchar deposit	4.1 ± 0.7–4.4 ± 0.4	K/Ar	Lippolt and Fuhrmann (1986)
K-feldspar	Andesite	Crven dol, Allchar deposit	4.2 ± 0.1	$^{40}Ar/^{39}Ar$	Troesh and Frantz (1992)
Amphibole	Latite	Allchar deposit	4.8 ± 0.2	$^{40}Ar/^{39}Ar$	Neubauer et al. (2009)
Biotite	Latite	Allchar deposit	4.6 ± 0.2–4.8 ± 0.2	$^{40}Ar/^{39}Ar$	Neubauer et al. (2009)
K-feldspar	Latite	Allchar deposit	3.3–4.0	$^{40}Ar/^{39}Ar$	Neubauer et al. (2009)
Biotite	Tuff	Vitačovo, Allchar deposit	5.1 ± 0.1–5.1 ± 0.1	$^{40}Ar/^{39}Ar$	Neubauer et al. (2009)
K-feldspar	-	Rudina, Allchar deposit	4.31 ± 0.02	$^{40}Ar/^{39}Ar$	Neubauer et al. (2009)
Sericite and K-feldspar	Sericite-quartz alteration zone	Allchar deposit	119.8 ± 1.2–125.1 ±1.8	$^{40}Ar/^{39}Ar$	Neubauer et al. (2009)

Abbreviations: Qtz = quartz

Table 2. Carbon and Oxygen Isotope Data of Country Rock, Gangue Minerals, and Fluid Inclusions from the the Allchar Au-As-Sb-Tl Deposit

Sample	Mineralogy	$\delta^{13}C$ (‰ V-PDB)	$\delta^{18}O$ (‰ V-SMOW)	Reference
1	Calcite	2.4	14.9	Volkov et al. (2006)
2	Calcite	3.4	28.7	Volkov et al. (2006)
3	Calcite	2.7	20.7	Volkov et al. (2006)
4	Calcite	3.1	26.2	Volkov et al. (2006)
5	Calcite	3.9	21.6	Volkov et al. (2006)
6	Calcite	2.0	24.1	Volkov et al. (2006)
ADP-232	Tertiary sanded dolomite	3.5	30.0	This study
100	Tertiary dolomite, barren	3.7	29.4	This study
Ad-823	Tertiary dolomite, barren	3.5	29.2	This study
Tl-Adit	Mineralized dolomite with orpiment	1.1	19.8	This study
TR-ADP-49	Triassic marble, barren	2.8	19.6	This study
Adit I	Mineralized Triassic marble with realgar	3.3	16.1	This study
Adit River	Late calcite with stibnite	4.7	13.5	This study
S2	Late calcite	0.7	10.4	This study
5NE 1/4	Late calcite within marble	–8.6	–4.5	This study
CD-7 orp	Fluid inclusions in orpiment	4.3	9.0	This study
SM-Adit bar	Fluid inclusions in barite	–4.2	10.4	This study

Abbreviations: V-PDB = Vienna-Pee Dee belemnite, V-SMOW = Vienna-standard mean ocean water

Table 3. Sulfur Isotope Data of Sulfides from the Allchar Au-As-Sb-Tl Deposit

Sample	Mineralogy	$\delta^{34}S$ (‰ V-CDT)	Reference	Sample	Mineralogy	$\delta^{34}S$ (‰ V-CDT)	Reference
Marc	Marcasite	–4.7	Jankovic (1993)	B1	Botryoidal marcasite/pyrite	–4.9	This study
Real/Orp max	Realgar/orpiment	–1.6	Jankovic (1993)				
Real/Orp min	Realgar/orpiment	–3.8	Jankovic (1993)	B2	Botryoidal marcasite/pyrite	–4.7	This study
Real/Orp mean	Realgar/orpiment	–2.2	Jankovic (1993)				
Stb max	Stibnite	0.4	Jankovic (1993)	Py1	Disseminated pyrite/marcasite	–3.2	This study
Stb min	Stibnite	–5.6	Jankovic (1993)				
Stb mean	Stibnite	–2.2	Jankovic (1993)	Py2	Disseminated pyrite/marcasite	–4.1	This study
Lor-823	Lorandite	–5.7	Frantz et al. (1994)				
Real-823	Realgar	–1.7	Frantz et al. (1994)	Py3	Disseminated pyrite/marcasite	–3.7	This study
Marc-823	Marcasite	–1.7	Frantz et al. (1994)				
Lor-817	Lorandite	–2.1	Frantz et al. (1994)	Py4	Disseminated pyrite/marcasite	–4.7	This study
Real-817	Realgar	–2.6	Frantz et al. (1994)				
Orp-817	Orpiment	–2.6	Frantz et al. (1994)	ADP-275	Disseminated pyrite/marcasite	–3.8	This study
Lor-800	Lorandite	–2	Frantz et al. (1994)				
Real-800	Realgar	–2.7	Frantz et al. (1994)	AI-9 py-1	Disseminated pyrite/marcasite	–4.7	This study
Orp-800	Orpiment	–2.2	Frantz et al. (1994)				
Lor-763	Lorandite	–2	Frantz et al. (1994)	AI-9 py-2	Disseminated pyrite/marcasite	–5.2	This study
Orp-763	Orpiment	–2.5	Frantz et al. (1994)				
14564	Stibnite	0.4	Volkov et al. (2006)	CD-5 orp	Orpiment	–2.4	This study
14565	Stibnite	–0.3	Volkov et al. (2006)	CD-7 orp	Orpiment	–2.9	This study
14566	Stibnite	–0.4	Volkov et al. (2006)	Tl-Adit orp A	Orpiment	–0.8	This study
14567	Stibnite	–4.7	Volkov et al. (2006)	Tl-Adit orp B1	Orpiment	–1.6	This study
14568	Stibnite	–5.6	Volkov et al. (2006)	Tl-Adit orp B2	Orpiment	–1.9	This study
14569	Stibnite	–1.8	Volkov et al. (2006)	AD-2 real	Realgar	–3.1	This study
14571	Stibnite	–5.2	Volkov et al. (2006)	Adit I real1	Realgar	–0.9	This study
14576	Stibnite	–3.6	Volkov et al. (2006)	Adit I real2	Realgar	–3.1	This study
16	Stibnite	–2.7	Volkov et al. (2006)	ADP-58A real1	Realgar	–4.2	This study
17	Stibnite	–2.7	Volkov et al. (2006)	ADP-58B real1	Realgar	–3.6	This study
14572	Realgar	–1.6	Volkov et al. (2006)	ADP-58A real2	Realgar	–4.4	This study
14573	Realgar	–3.8	Volkov et al. (2006)	ADP-58B real2	Realgar	–3.8	This study
20	Realgar	–0.2	Volkov et al. (2006)	ALH-3 real1	Realgar	–0.5	This study
21	Realgar	–1.5	Volkov et al. (2006)	ALH-3 real2	Realgar	–0.1	This study
14574	Orpiment	–3.7	Volkov et al. (2006)	Alsh real	Realgar	–2.1	This study
14570	Marcasite	–6.8	Volkov et al. (2006)	Highgr. real	Realgar	–0.7	This study
18	Marcasite	–0.7	Volkov et al. (2006)	A-1 stb	Stibnite	–4.7	This study
19	Marcasite	–0.9	Volkov et al. (2006)	ADP-275 stb	Stibnite	–2.5	This study
Al-9 marc	Botryoidal marcasite/pyrite	–5.5	This study	Al-11	Stibnite	–3.7	This study
				ALP-21	Stibnite	–2.9	This study
C.a. riv1	Botryoidal marcasite/pyrite	–8	This study	Alsh SbS3	Stibnite	–4.9	This study
				Alsh Stb blad	Stibnite	–4.9	This study
C.a. riv2	Botryoidal marcasite/pyrite	–9.8	This study	C.a. riv stb	Stibnite	–2.4	This study
				Highgr. stb	Stibnite	–3.5	This study

Abbreviations: V-CDT = Vienna-Canyon Diablo Troilite

Microthermometric measurements of fluid inclusions within transparent minerals were performed at the University of Zagreb. Double polished, ~0.5-mm-thick, transparent mineral wafers were used. Measurements were carried out on a Linkam THMS 600 stage mounted on an Olympus BX 51 microscope using 10× and 50× Olympus long-working distance objectives for visible light. Two synthetic fluid inclusion standards (SYN FLINC; pure H_2O and mixed H_2O-CO_2) were used to calibrate the equipment. The precision of the system was ±2.0°C for homogenization temperatures and ±0.2°C in the temperature range between –60° and 10°C.

Geochronology

The geochronology data obtained from altered and mineralized samples as well as associated volcanic rocks are summarized in Table 1. The K/Ar, $^{40}Ar/^{39}Ar$, and fission track ages suggest that hydrothermal activity was contemporaneous with Pliocene calc-alkaline to shoshonitic volcanism (~5 Ma). Exceptions are $^{40}Ar/^{39}Ar$ data collected on sericite and K-feldspar from a sericite-quartz alteration zone spatially associated with Tl mineralization that yielded Cretaceous ages between 119.8 ± 1.2 and 125.1 ± 1.8 Ma (Neubauer et al., 2009). The paragenetic and geochemical relationships, described in the hydrothermal alteration and mineralization sections, suggest that this alteration zone was overprinted by the Pliocene hydrothermal fluids that introduced Au, Sb, As, and Tl.

Lithogeochemistry

The mineralization at the Allchar Au-As-Sb-Tl deposit is spatially associated with Pliocene hypabyssal intrusions and volcanic rocks that are well exposed throughout the Kozuf Mountains (Janković et al., 1997; Yanev et al., 2008; Boev and Jelenković, 2012). These rocks are felsic to intermediate in composition (52 and 66 wt % SiO_2; Electronic App. 1) with high-K calc-alkaline to shoshonitic affinities (Fig. 8A-C). In the major element classification of Le Bas et al. (1986) and the trace element classification of Hastie et al. (2007), the volcanic rocks of the Kozuf Mountains plot in the field of basaltic trachyandesite, trachyandesite, andesite, and trachyte/trachydacite (Fig. 8A, C). Their TiO_2, MgO, Fe_2O_3, and MnO contents show pronounced negative correlations with the SiO_2 concentration. Aluminum oxide, K_2O, and P_2O_5 do not show clear trends, and Na_2O shows a positive correlation (Fig. 9). The Pliocene igneous rocks of the area are mostly characterized by high Sr/Y and La/Yb ratios (Fig. 8D, E). Their multielement patterns show high large ion lithophile element/high field strength element (LILE/HFSE) ratios with strong depletions of Nb, Ta, and Ti and pronounced U and Pb peaks (Fig. 8F). The chondrite-normalized rare earth element (REE) patterns display an enrichment in light rare earth elements (LREEs) compared to heavy rare earth elements (HREEs) and weak to pronounced negative Eu anomalies (Fig. 8G). The lithogeochemical characteristics of igneous rocks associated with the Allchar Au-As-Sb-Tl deposit (high Sr/Y, La/Yb, LILE/HFSE, and LREE/HREE ratios; depletions in Nb, Ta, and Ti; and enrichment in U and Pb) are characteristic of subduction-related magmatism (e.g., Stolz et al., 1996; Gao et al., 2007; Booden et al., 2011). Tertiary igneous rocks with identical geochemical signatures have been described at numerous localities along the Vardar zone and the Serbo-Macedonian massif of the Balkan Peninsula (Fig. 1). They are usually associated with base and/or precious metal occurrences that formed in an extensional tectonic regime (e.g., Crnac Pb-Zn-Ag deposit, Borojević Šoštarić et al., 2012; Buchim Cu-Au deposit, Lehmann et al., 2013; Trepca Pb-Zn-Ag deposit, Strmić Palinkaš et al., 2016). The late Tertiary igneous rocks of the Balkan Peninsula have generally been

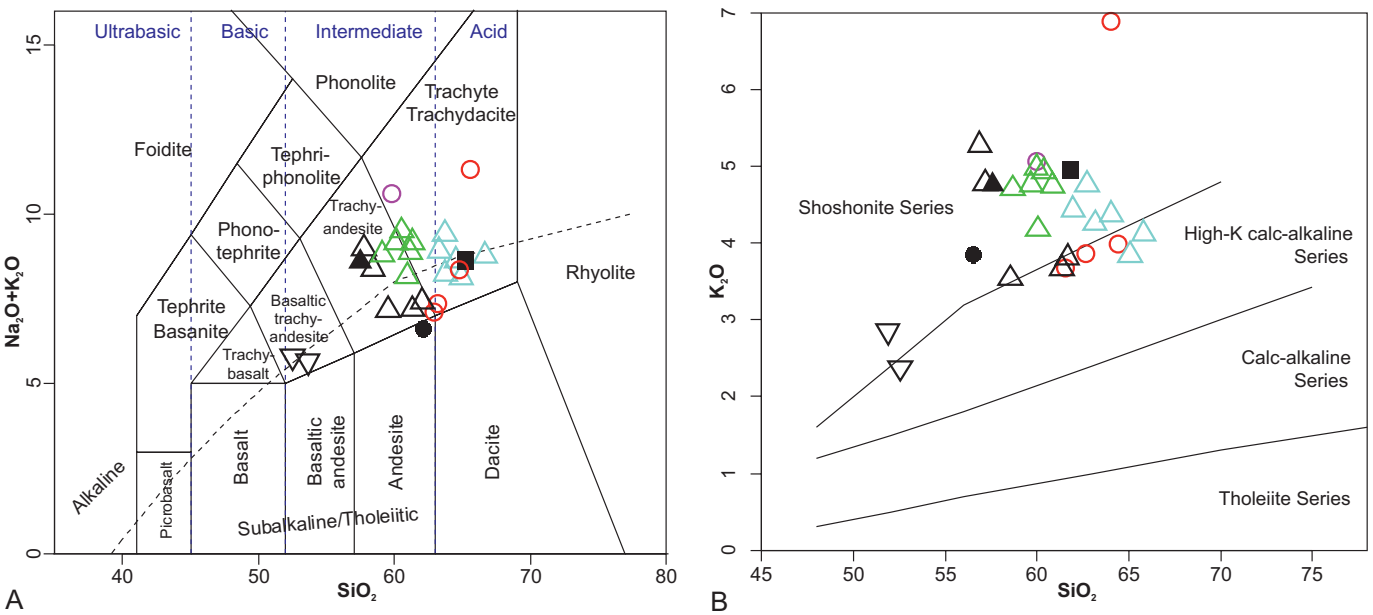

Fig. 8. Lithogeochemical data obtained from the Pliocene magmatic rocks spatially associated to the Allchar Au-As-Sb-Tl deposit (Janković et al., 1997; Yanev et al., 2008; Boev and Jelenković, 2012). (A) Total alkali vs. SiO_2 diagram (according to Le Bas et al., 1986). (B) K_2O vs. SiO_2 classification diagram (according to Peccerillo and Taylor, 1976). (C) Th vs. Co classification diagram (according to Hastie et al., 2007). (D) Sr/Y vs. Y classification diagram (according to Castillo et al., 1999). (E) $(La/Yb)_N$ vs. Yb_N classification diagram (according to Martin, 1999). (F) Primitive mantle-normalized multivariation diagram (according McDonough and Sun, 1995). G. Chondrite-normalized rare earth element pattern (according to Boynton, 1984).

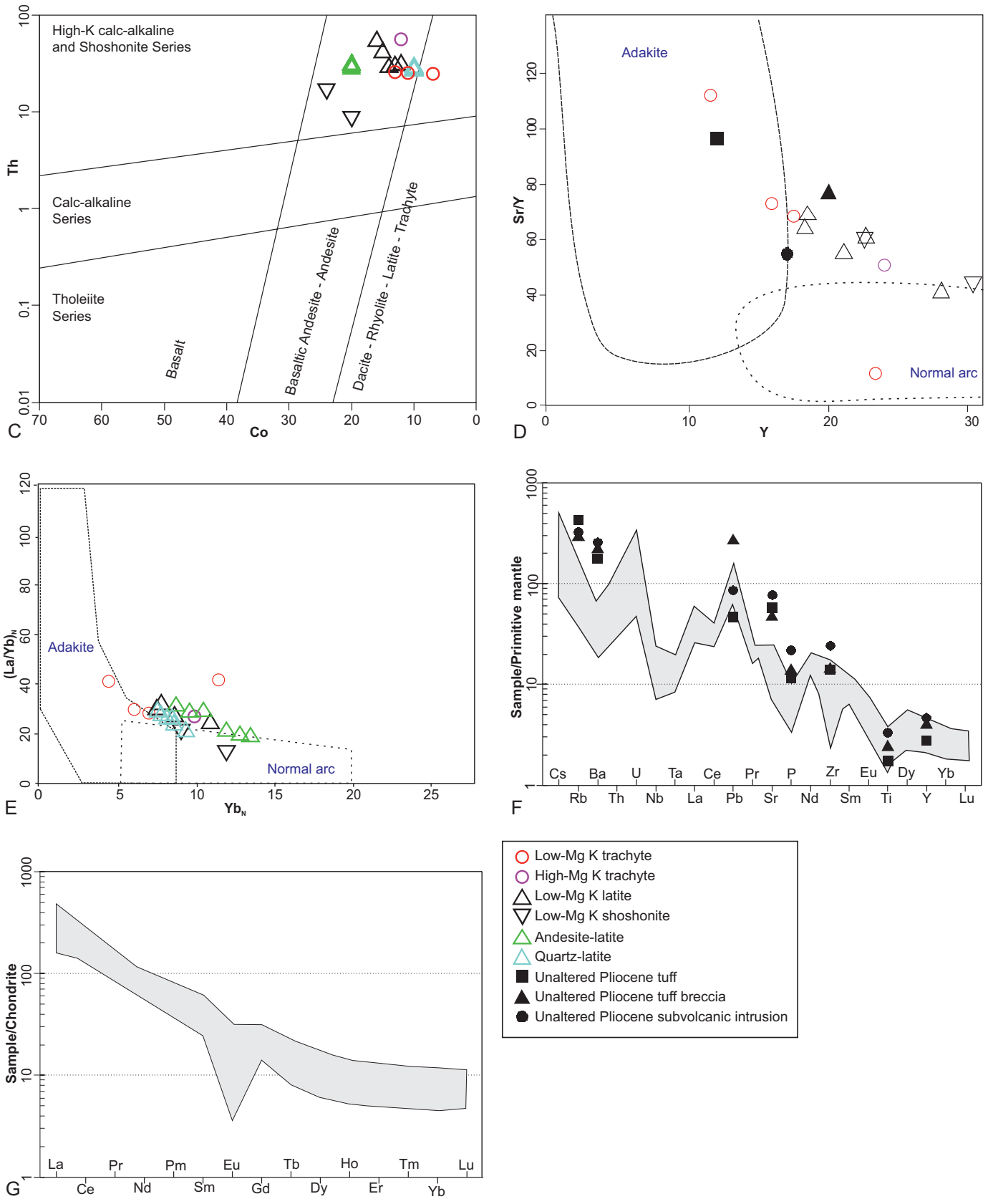
High-K calc-alkaline
and Shoshonite Series
Calc-alkaline
Series
Tholeiite
Series
Basalt
Basaltic Andesite - Andesite
Dacite - Rhyolite - Latite - Trachyte
Th
Co
C
Adakite
Normal arc
Sr/Y
Y
D
(La/Yb)N
YbN
E
Sample/Primitive mantle
Cs Ba U Ta Ce Pr P Zr Eu Y Dy Yb
Rb Th Nb La Pb Sr Nd Sm Ti Y Lu
F
Sample/Chondrite
La Pr Pm Eu Tb Ho Tm Lu
Ce Nd Sm Gd Dy Er Yb
G
Low-Mg K trachyte
High-Mg K trachyte
Low-Mg K latite
Low-Mg K shoshonite
Andesite-latite
Quartz-latite
Unaltered Pliocene tuff
Unaltered Pliocene tuff breccia
Unaltered Pliocene subvolcanic intrusion

Fig. 8. *(Cont.)*

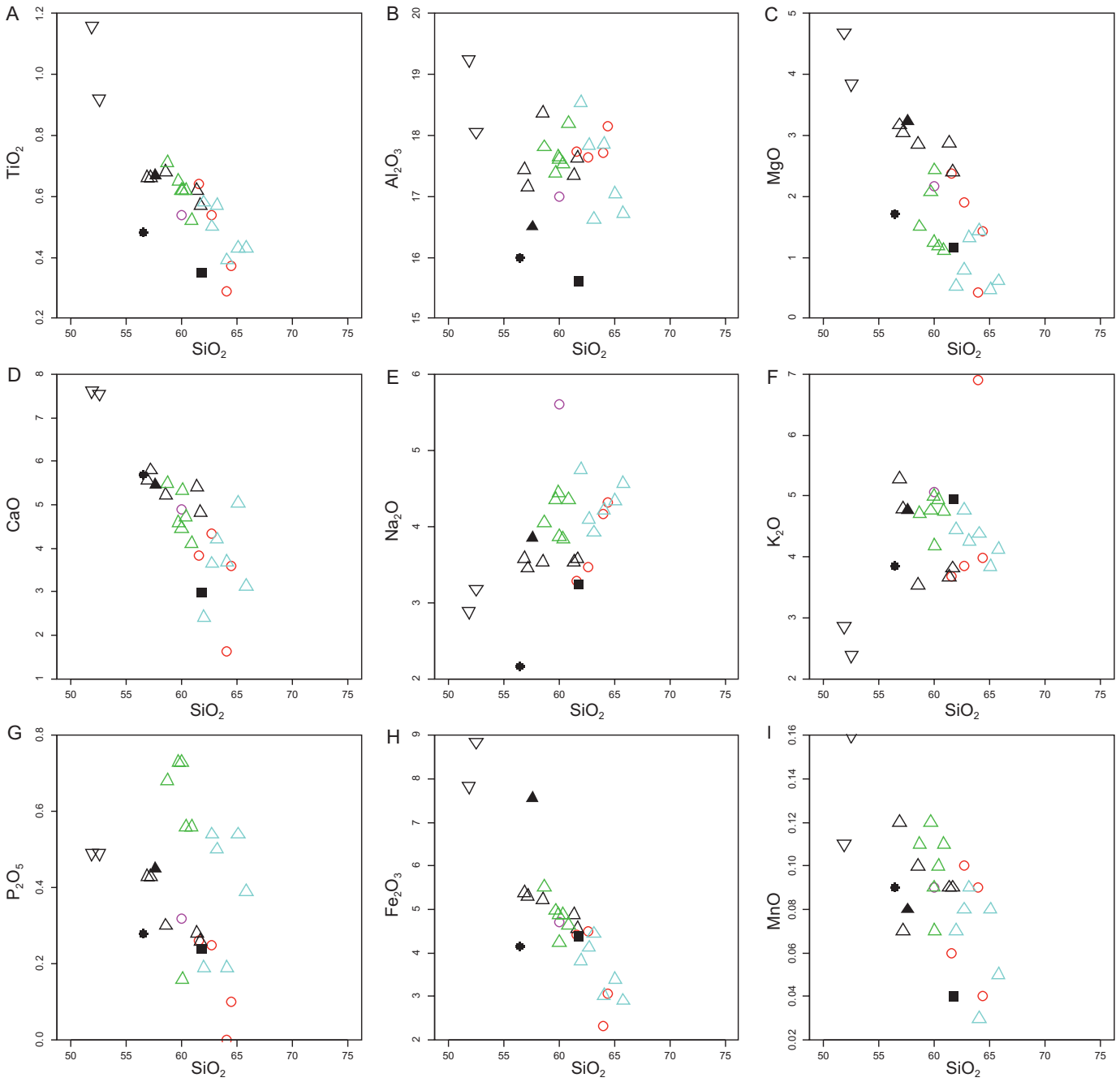

Fig. 9. Harker diagrams illustrating (A) TiO_2, (B) Al_2O_3, (C) MgO, (D) CaO, (E) Na_2O, (F) K_2O, (G) P_2O_5, (H) Fe_2O_3, and (I) MnO variations for the Pliocene igneous rocks spatially associated with the Allchar Au-As-Sb-Tl deposit. Symbols as in Figure 8.

attributed to postcollisional collapse of the Dinaride orogen followed by extension of the Pannonian (Miocene) and Aegean areas (Eocene-Pliocene) (Cvetković et al., 2000, 2004; Prelević et al., 2005; Jolivet and Brun, 2010; Koroneos et al., 2011; Schefer et al., 2011; Borojević Šoštarić et al., 2012; Lehmann et al., 2013; Melfos and Voudouris, 2017). Available Sr and Nd isotope data from the Kozuf Mountains area ($^{87}Sr/^{86}Sr$ = 0.7085–0.7093; $^{143}Nd/^{144}Nd$ = 0.51230–0.51233) suggest significant assimilation of continental crust (Yanev et al., 2008).

The mineralization at the Allchar Au-As-Sb-Tl deposit is hosted by various rock types including Triassic marble, Tertiary dolomite, Tertiary tuff, and the basal unconformity between Tertiary and Triassic rocks (Janković, 1993; Percival and Radtke, 1994). The whole-rock geochemical data obtained on host rocks and their unaltered equivalents published by Percival and Radtke (1994) are summarized in Electronic Appendix 1. Isocon analysis (Grant, 2005) has been applied to mineralized rocks and their unaltered equivalents (Fig. 10).

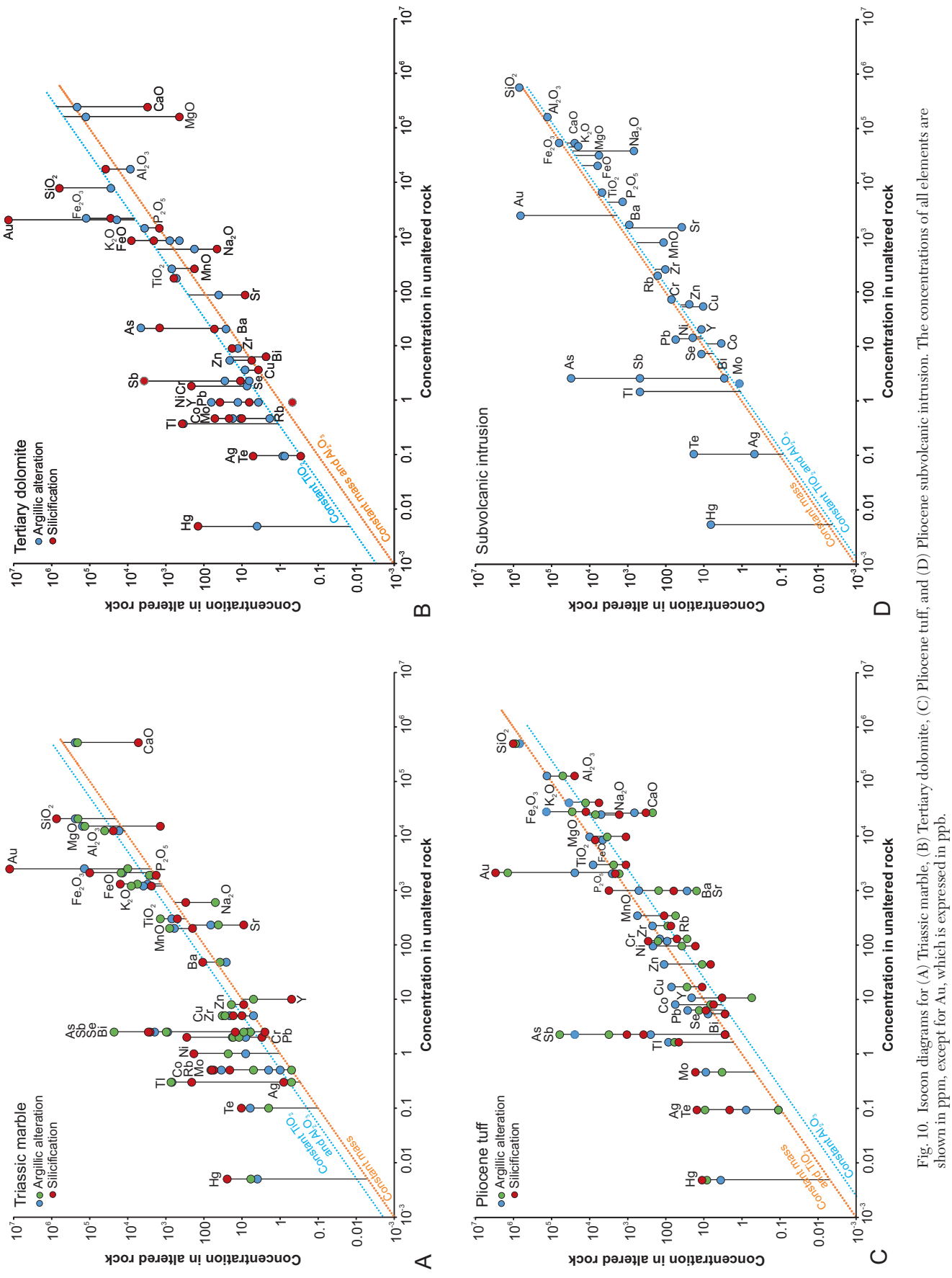

Fig. 10. Isocon diagrams for (A) Triassic marble, (B) Tertiary dolomite, (C) Pliocene tuff, and (D) Pliocene subvolcanic intrusion. The concentrations of all elements are shown in ppm, except for Au, which is expressed in ppb.

In silicified and argillized Triassic marble, TiO_2, Al_2O_3, MnO, Ag, Bi, Pb, Cu, and Zn are relatively immobile and Ca, Na, Sr, and Y are depleted (Fig. 10A). Magnesium is depleted in silicified rocks and introduced in argillized rocks. Although Au, Co, Cr, Fe, Hg, Ni, Sb, Se, Te, and Zr are introduced in each alteration type, silicified rocks are more enriched in these elements than argillized rocks. In contrast, argillic alteration is more strongly enriched in Tl, Rb, and K_2O than silicified rocks (Fig. 10A).

In Tertiary dolomite, argillic alteration is associated with the introduction of Fe_2O_3, As, Tl, Pb, Sb, Hg, and Ag and depletion of CaO, MgO, Al_2O_3, Na_2O, K_2O, and Sr (Fig. 10B); TiO_2 is immobile. In contrast, silicification is associated with depletion of CaO, MgO, Na_2O, MnO, and Sr and introduction of SiO_2, K_2O, Fe_2O_3, Rb, As, Sb, Cr, Tl, and Hg (Fig. 10B).

In Pliocene tuff, altered rock is depleted in CaO, Na_2O, Ba, and Sr and enriched in Hg, Te, Mo, As, Sb, Tl, Ag, and Au (Fig. 10C). The Au, Ag, and Hg enrichments are more pronounced in silicified tuff than in argillized tuff, whereas Tl is more enriched in argillized tuff (Fig. 10C).

In a Pliocene subvolcanic intrusion, the altered rock is depleted in CaO, K_2O, MgO, FeO, P_2O_5, MnO, Cu, Zn, Sr, and Co. It is enriched in Hg, Te, Tl, Ag, Au, As, and Sb. Silica, Al_2O_3, TiO_2, Cr, Ni, Bi, and Mo are relatively immobile (Fig. 10D).

In all altered host rocks (Fig. 10), Au/Ag ratios are relatively high (100–10,000) and the abundance of base metals is low (Cu + Zn + Pb + Mo + Co + Ni <1,000 ppm), suggesting that the solubility of Ag and base metals was suppressed by a high activity of H_2S in ore fluids (e.g., Hofstra and Cline, 2000). The isocon diagrams reveal hydrothermal solutions at the Allchar deposit introduced much more Fe, Mg, and K than hydrothermal fluids in Nevada Carlin-type gold deposits (e.g., Hofstra and Cline, 2000).

Mineral Chemistry

LA-ICP-MS multielement analyses of pyrite grains in mineralized samples from the Allchar Au-As-Sb-Tl deposit reveal that the grains are enriched in Mn, Te, Sn, Cu, W, Cs, Pb, and Au without significant chemical zonation (Fig. 11A, B, D). On the Au vs. As diagram, some of the pyrite samples plot in the Carlin pyrite field, but the majority are in the diagenetic pyrite or intrusion-related pyrite fields. All data plot below the Au saturation line (Fig. 12) with Au concentrations less than 1,000 ppm.

Stibnite is enriched in Se and Te and has detectable amounts of Tl, Hg, Ag, and Pb (Fig. 11E, F). Some stibnite crystals have rims with elevated concentrations of As and Cu (Fig. 11E). Orpiment and lorandite contain significant amounts of Sn, Pb, Sb, and Hg (Fig. 11G). Realgar shows a zonal trace element distribution with cores enriched in Sb and Te and rims enriched in Tl and Pb. It also contains detectable concentrations of Sn and Hg (Fig. 11C).

The geochemical signature characterized by elevated concentrations of Se, Te, Hg, As, Sb, Cu, Sn, Pb, Mn, and Cs in these sulfides may be indicative of a magmatic source. It is also possible that Pb, Sn, and W were leached from underlying continental crust, whereas Mn could be derived from ophiolites that occur near the Allchar deposit (Fig. 2).

Lead Isotope Data

Lead isotope compositions of sulfide minerals and country rocks associated with the mineralization at the Allchar Au-As-Sb-Tl deposit are listed in Electronic Appendix 2 and plotted in Figure 13. The Pb isotope compositions of two Pliocene subvolcanic intrusions are very similar to one another and plot in the mature arc or upper continental crust fields (Fig. 13). They mostly overlap with the average values obtained for galena and volcanic rocks from the Belo Brdo Pb-Zn hydrothermal deposit in Kosovo (Veselinovic-Williams, 2011) and the average values for galena from the Inkaya Cu-Pb-Zn prospect, northwestern Turkey (Ozen and Arik, 2015). Both the Belo Brdo deposit and the Inkaya prospect have been interpreted as products of voluminous postcollisional calc-alkaline to ultrapotassic magmatism that followed closure of the Vardar ocean in Oligocene to early Miocene time (Erkul and Erkul, 2010; Veselinovic-Williams, 2011; Ozen and Arik, 2015).

In contrast, sulfide minerals are similar to Tertiary dolomite, and most are widely scattered across the oceanic island volcanic rock field on the ^{208}Pb vs. ^{206}Pb diagram and the upper continental crust field on the ^{207}Pb vs. ^{206}Pb diagram. The distribution of data suggests that the Pb in ore minerals was derived primarily from the country rocks.

Stable Isotope Studies

To determine the source of water, CO_2, and H_2S in ore fluids, new and previously published stable isotope data (δD, $\delta^{18}O$, $\delta^{13}C$, $\delta^{34}S$) on hydrothermal minerals and fluid inclusions were synthesized. Hydrogen and oxygen isotope data were used to constrain the source of water and to estimate water-rock ratios. Sulfur isotope data reflect the source of H_2S and, in samples where isotopic equilibrium was achieved, the temperature of mineral precipitation. Carbon and oxygen isotopes can potentially discriminate between sedimentary carbonates, organic matter, and magmatic sources of CO_2.

The δD and $\delta^{18}O$ data obtained from gangue minerals and fluid inclusions are listed in Table 4. The calculated and measured δD_{H_2O} and $\delta^{18}O_{H_2O}$ values define a triangular field that extends from the primary magmatic water box toward the meteoric water line (Fig. 14). The data indicate that magmatic fluid mixed with exchanged meteoric water at deep levels and with unexchanged meteoric water at shallow levels in the system (Fig. 14).

The $\delta^{13}C$ and $\delta^{18}O$ values of barren and altered host rocks, vein calcite, and fluid inclusion extracts are listed in Table 4. The $\delta^{13}C$ value of barren Triassic marble is within the range of Phanerozoic marine carbonates (Veizer and Hoefs, 1976), and its $\delta^{18}O$ value is consistent with Triassic marine carbonate values (Claypool et al., 1980), indicating that the original isotopic composition of the Triassic limestone was not significantly disturbed by metamorphic recrystallization (Fig. 15). The $\delta^{13}C$ values of barren Tertiary dolomite are similar to Phanerozoic marine carbonate (Veizer and Hoefs, 1976), but their $\delta^{18}O$ values are higher than average Tertiary marine carbonate (Fig. 15). The calculated isotopic composition of fluid in equilibrium with altered and mineralized marble and dolomite, vein calcite, and inclusion fluid extracted from orpiment and barite defines a field that extends between three sources: carbonate rock-buffered fluid, magmatic fluid, and meteoric

water (Fig. 15). The calcite vein with the lowest $\delta^{18}O$ and $\delta^{13}C$ values may contain CO_2 produced by the oxidation of organic carbon in the host rocks.

The sulfur isotope data are summarized in Table 3 and Figure 16. The absence of hypogene sulfate minerals and dissolution of calcite and dolomite as well as precipitation of marcasite and kaolinite point to a low redox potential and low pH values of hydrothermal fluids associated with deposition of siliceous Au mineralization. Under such Eh-pH conditions, H_2S predominates over other sulfur species. Early-stage

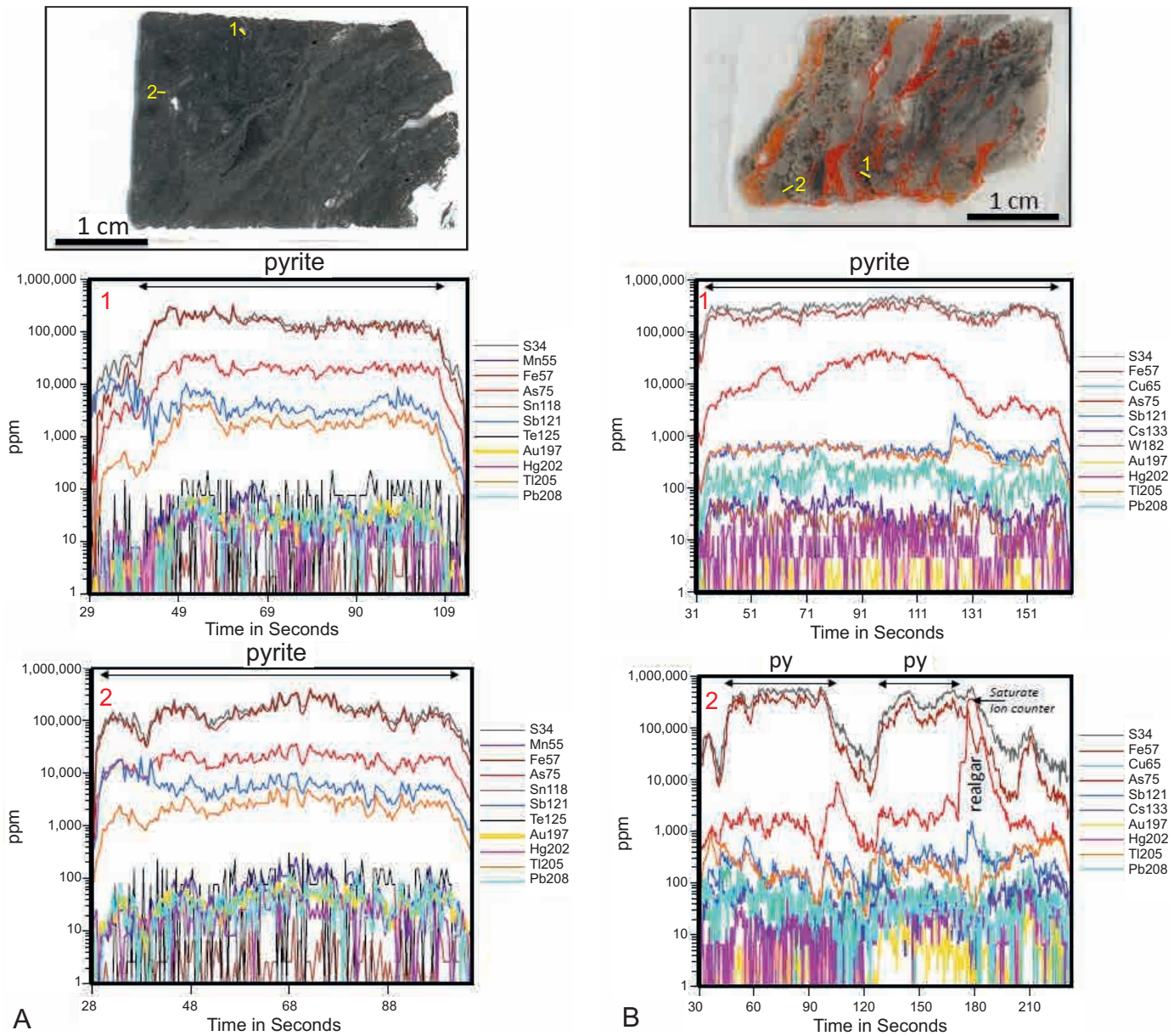

Fig. 11. Laser ablation-inductively coupled plasma-mass spectrometry multielement profiles. (A) Profiles across a pyrite crystal in the mineralized sample (AD-9; disseminated pyrite/marcasite; $\delta^{34}S_{Py}$ = –4.7 to –5.2‰). Profile 1 shows pyrite enriched in Mn, Te, and Sn. The left side of the profile with higher Sb and lower S, Fe, As, and Tl concentrations may indicate the presence of tetrahedrite. Profile 2 shows pyrite enriched in Mn, Te, and Sn. (B) Profiles across a pyrite crystal in an As ore sample (AD-2). Profile 1 shows pyrite enriched in Cu, W, Cs, and Pb. Profile 2 shows two pyrite crystals enriched in Cu, Cs, and Pb. (C) Profile across realgar in an As ore sample (AD-2; $\delta^{34}S_{Rlg}$ = –3.1‰). Realgar contains zones enriched in Sb and Te and rims enriched in Tl and Pb. It also contains Sn and Hg. (D) Profile across two pyrite crystals in an As ore sample (AD-1). Pyrite is enriched in Te, W, and Pb. (E) Profile across Se- and Te-bearing stibnite crystal in a quartz vein (FI-2). The rims are enriched in As and Cu. The flat blue line shows that Sb saturated the ion counter. (F) Profile across two stibnite crystals associated with drusy quartz (Sample ALP-21; $\delta^{34}S_{Sb}$ = –2.9‰). Arsenic, Se, and Te are the main trace elements, and Tl, Hg, Ag, and Pb have been detected. The flat blue line shows that Sb saturated the ion counter. (G) Profile across orpiment and lorandite crystals (Sample CD-5; $\delta^{34}S_{Orp}$ = –2.4‰). Lorandite contains more Pb, Sb, and Hg than orpiment. Both minerals contain elevated concentrations of Sn. The flat red and orange lines show that As and Tl saturated the ion counter. Abbreviations: Asp = arsenopyrite, Lor = lorandite, Orp = orpiment, Py = pyrite, Rlg = realgar.

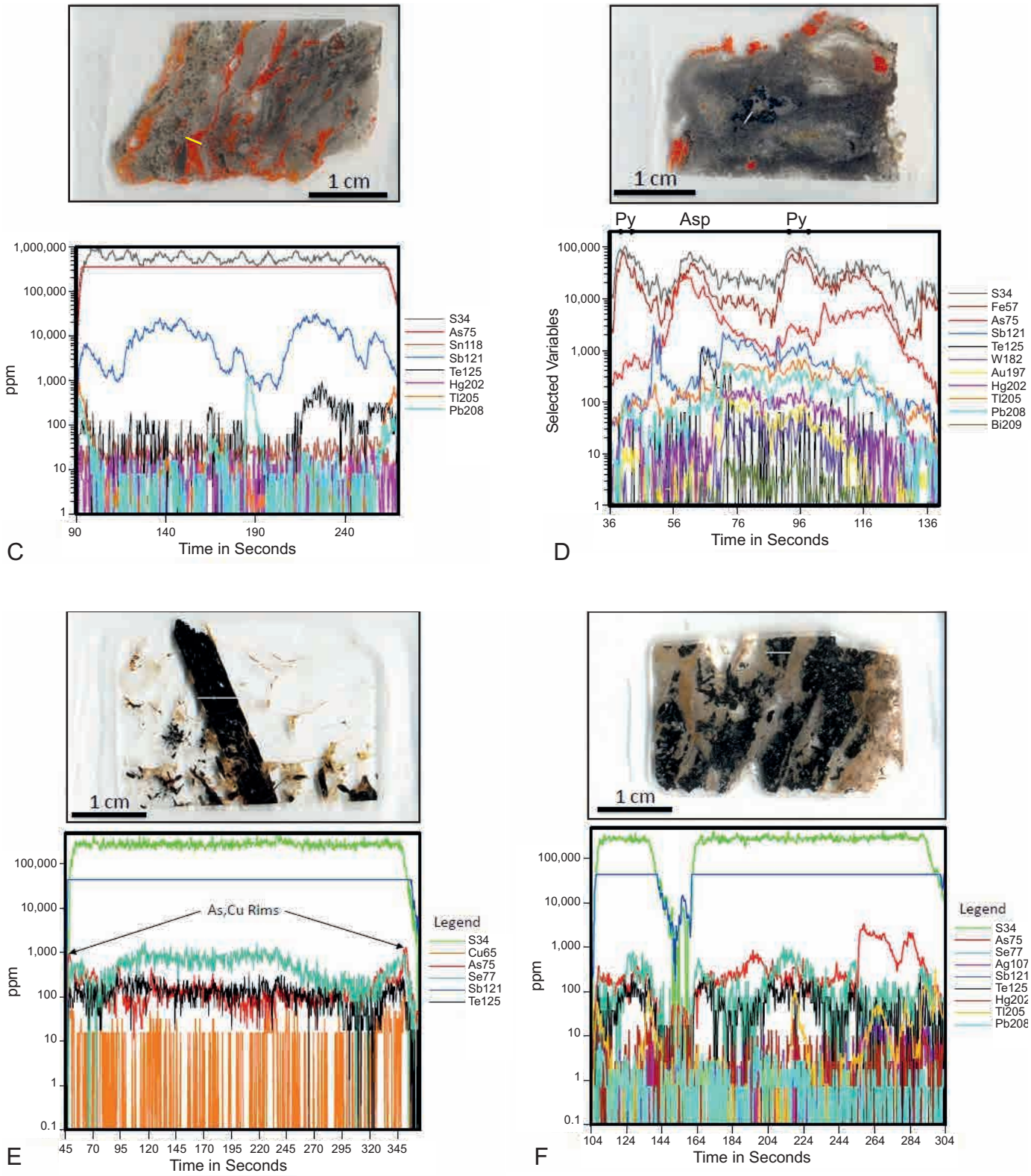
1 cm
1,000,000
100,000
10,000
1,000
100
10
1
ppm
90
140
190
240
Time in Seconds
S34
As75
Sn118
Sb121
Te125
Hg202
Tl205
Pb208
C
Py
Asp
Py
100,000
10,000
1,000
100
10
1
Selected Variables
36
56
76
96
116
136
Time in Seconds
S34
Fe57
As75
Sb121
Te125
W182
Au197
Hg202
Tl205
Pb208
Bi209
D
1 cm
100,000
10,000
1,000
100
10
1
0.1
ppm
As,Cu Rims
45
70
95
120
145
170
195
220
245
270
295
320
345
Time in Seconds
Legend
S34
Cu65
As75
Se77
Sb121
Te125
E
1 cm
100,000
10,000
1,000
100
10
1
0.1
ppm
104
124
144
164
184
204
224
244
264
284
304
Time in Seconds
Legend
S34
As75
Se77
Ag107
Sb121
Te125
Hg202
Tl205
Pb208
F

Fig. 11. *(Cont.)*

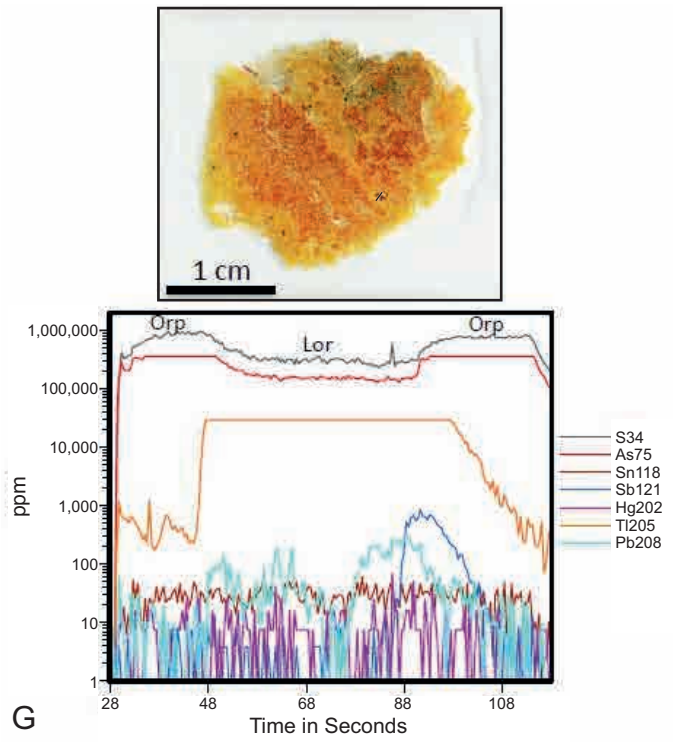

Fig. 11. *(Cont.)*

disseminated pyrite and marcasite have calculated $\delta^{34}S_{H_2S}$ values between –5.0 and –7.0‰, suggesting that H_2S was initially derived from diagenetic pyrite in sedimentary rocks (Ohmoto and Rye, 1979). In contrast, stibnite, orpiment, and realgar have calculated $\delta^{34}S_{H_2S}$ values between –2.7 and 2.6‰, reflecting a strong input of magmatic H_2S during the main mineralization stage. Late-stage botryoidal pyrite and marcasite, depleted in $\delta^{34}S$ and with calculated $\delta^{34}S_{H_2S}$ values between –6.5 and –11.6‰, point to diminishing influence of magmatic volatiles and predomination of H_2S from sedimentary sources during the late-mineralization stage. Presence of barite in the later stages of the mineralization indicates increase in oxygen fugacity that could have contributed to partial oxidation of bulk sulfur and resulted in fractionation of isotopically light sulfide from isotopically heavy sulfate (e.g., Ohmoto, 1972; Kesler et al.,1981).

Fluid Inclusion Studies

Microthermometric measurements of fluid inclusions in various minerals from different stages of ore deposition in the Allchar Au-As-Sb-Tl deposit document changes in the temperature and salinity of hydrothermal fluids. Fluid inclusions were classified as primary, pseudosecondary, or secondary according to petrographic features proposed by Roedder (1984).

Quartz crystals selected from siliceous Au mineralization host several generations of two-phase, liquid + vapor fluid inclusions, but only primary inclusions were large enough to allow reliable microthermometric measurements (Fig. 17A). The uniform degree of fill (F) around 0.85 suggests entrapment of a single-phase fluid. The great majority of the fluid inclusions have first melting temperatures (eutectic temperature, T_e) between –44° and –58°C (Fig. 18A) that are characteristic of the H_2O-NaCl-$CaCl_2$ ± $MgCl_2$ system. Final melting temperature of hydrohalite ($T_{m\,hyd1}$) was recorded in the temperature interval between –24.2° and –42.0°C (Fig. 18B). Ice melting temperatures ($T_{m\,ice}$) from –2.4° to –18.1°C (Fig. 18C) correspond to salinities between 4 and 21.3 wt % NaCl equiv. Homogenization (T_h) by vapor disappearance occurred from

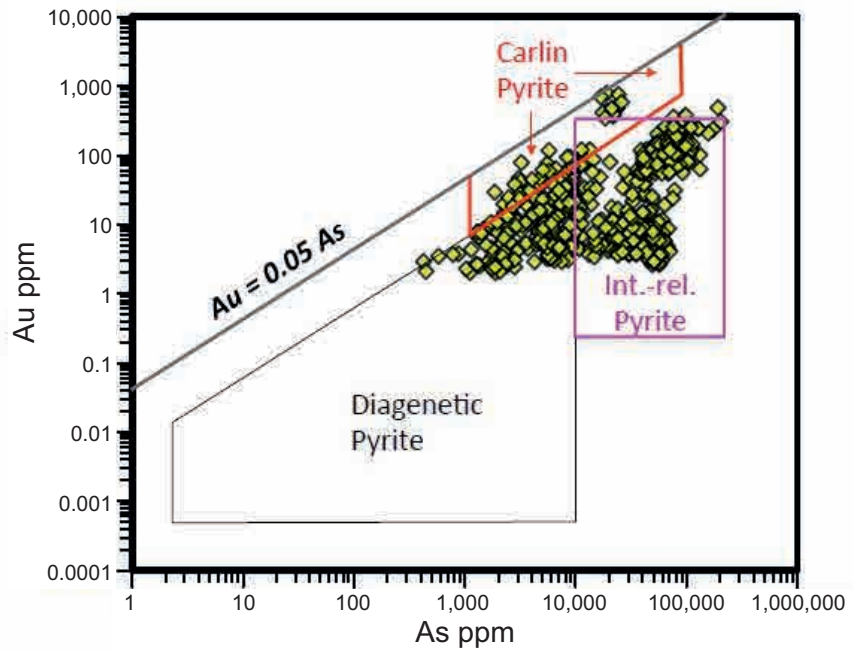

Fig. 12. Au vs. As plot based upon laser ablation-inductively coupled plasma-mass spectrometry analyses of pyrite in the Allchar mineralized samples. Most of the data plot in the diagenetic pyrite or intrusion-related (Int.-rel.) pyrite fields. Some of the data plot in the Carlin pyrite field. All data plot below the Au saturation line of Reich et al. (2005). Fields adapted from Large et al. (2011).

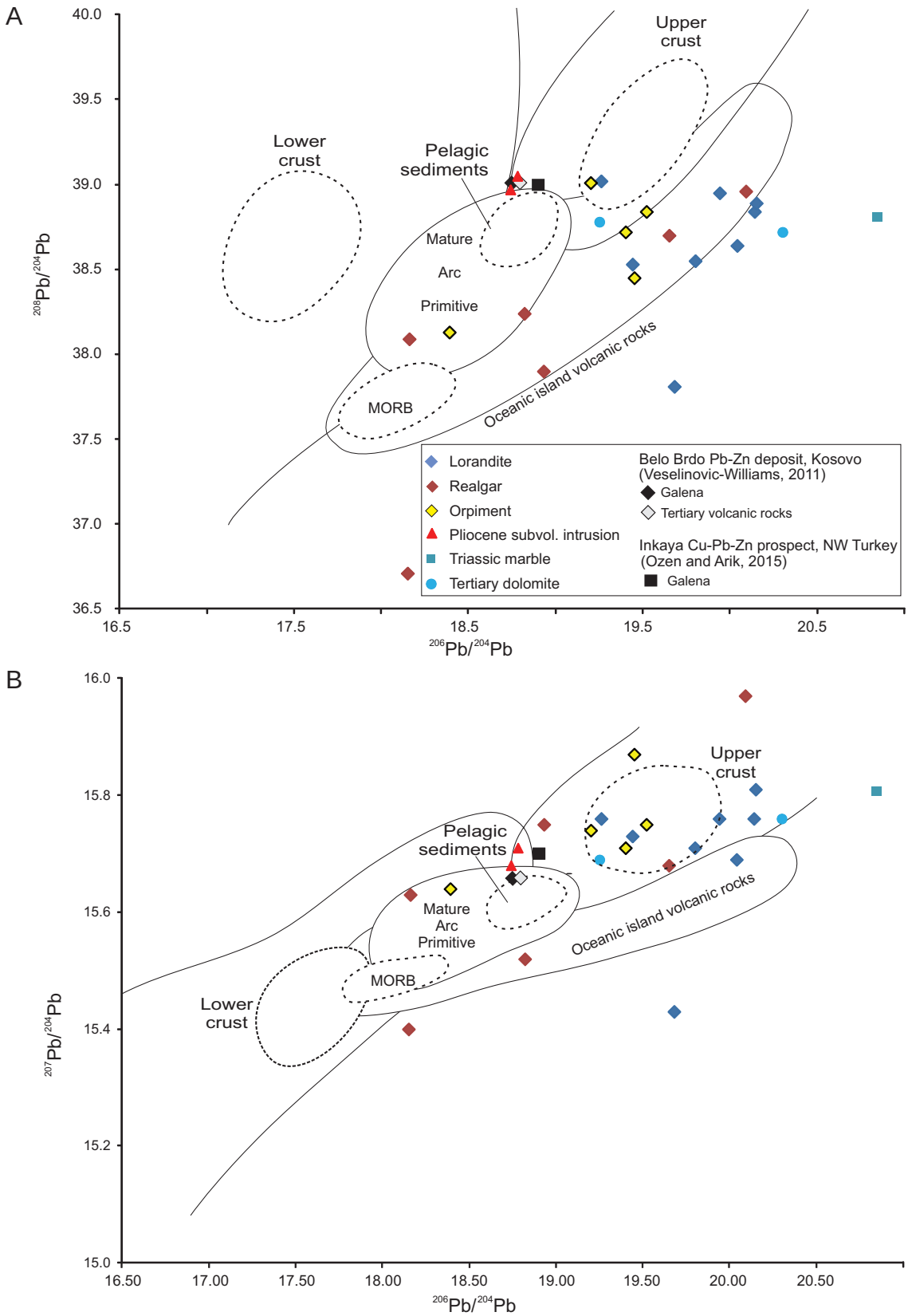

Fig. 13. (A) $^{208}Pb/^{204}Pb$ vs. $^{206}Pb/^{204}Pb$ and (B) $^{208}Pb/^{204}Pb$ vs. $^{207}Pb/^{204}Pb$ diagrams for selected country rocks and ore minerals at the Allchar Au-As-Sb-Tl deposit (Frantz et al., 1994), compared with average values for data published from the Belo Brdo Pb-Zn hydrothermal deposit (Veselinovic-Williams, 2011) and the Inkaya Cu-Pb-Zn prospect (Ozen and Arik, 2015). Pb isotope composition of fields adapted from Zartman and Doe (1981). Abbreviations: MORB = mid-ocean ridge basalt.

Table 4. Hydrogen and Oxygen Isotope Data of Country Rock, Gangue Minerals, and Fluid Inclusions from the Allchar Au-As-Sb-Tl Deposit

Sample	Mineralogy	δD_{H_2O} (‰ V-SMOW)	$\delta^{18}O_{mineral}$ (‰ V-SMOW)	$\delta^{18}O_{H_2O}$ (‰ V-SMOW)	Reference
AD-2	Fluid inclusions, realgar	–99			This study
SM-Adit	Fluid inclusions, barite	–97	10.4	2.6	This study
CD-7	Fluid inclusions, orpiment	–75		9.0	This study
5NE 1/4	Fluid inclusions, late calcite	–114	–4.5	–12.3	This study
FI-2	Fluid inclusions, milky quartz vein	–71	8.0	–3.6	This study
AD-2	Jasperoid		11.5	–0.1	This study
AD-2	Quartz		8.6	–3	This study
ADP-275	Jasperoid		10.7	–0.9	This study
ADP-275	Quartz		8.2	–3.4	This study
ADP-145	Jasperoid		10.4	–1.2	This study
AI-1	Quartz		10.4	–1.2	This study
High gr.	Jasperoid		9.6	–2	This study
ALP-21	Quartz		9.9	–1.7	This study
AI-9	Jasperoid		11.5	–0.1	This study
AI-11	Jasperoid		10.3	–1.3	This study

Abbreviations: V-SMOW = Vienna-standard mean ocean water

131° to 200°C (Fig. 18D). Several fluid inclusions nucleate a recognizable clathrate phase that melted between –0.5° and 3°C, suggesting the presence of CO_2 and salinities between 12.6 and 16 wt % NaCl equiv. Homogenization temperatures for this type of fluid inclusion were recorded between 185° and 202°C.

The physicochemical characteristics of mineralizing fluids associated with stibnite-bearing jasperoids were estimated from primary fluid inclusions hosted by jasperoid, quartz, and rare calcite crystals (Fig. 18). Jasperoid hosts aqueous-carbonic and hydrocarbon-bearing fluid inclusions (Fig. 17B). At room temperature, the aqueous-carbonic inclusions contain two immiscible liquids and a vapor phase. Melting of clathrates occurred from 2.4° to 7.0°C corresponding to salinity between 6.0 and 13.5 wt % NaCl equiv. The CO_2

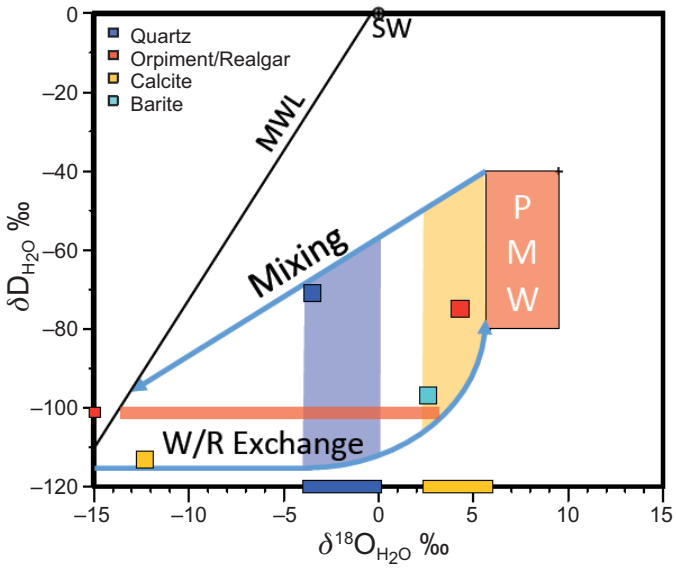

Fig. 14. Isotopic composition of water in equilibrium with, or extracted from, hydrothermal minerals relative to seawater (SW), meteoric water line (MWL) and primary magmatic water (PMW). Mixing and water/rock (W/R) exchange lines are shown in blue. The results suggest the deposit formed from mixtures of magmatic water and variably exchanged meteoric water.

homogenization to vapor phase is recorded between 31.0° and 33.0°C. Total homogenization to liquid phase was recorded between 102° and 125°C (Fig. 18).

The hydrocarbon-bearing inclusions contain one or more immiscible liquids or solid phases (Fig. 17C). They remain unfrozen at the minimum fluid inclusion stage temperature of –180°C. During subsequent heating, the only recorded change was a reduction in size or shape of some of the components without complete phase transitions. None of these inclusions homogenized before decrepitation, which occurred at temperatures from 170° to 180°C. Ultraviolet fluorescence of hydrocarbon-bearing fluid inclusions is in yellow and green colors, suggesting immature organic matter (e.g., Hagemann and Hollerbach, 1986; McLimans, 1987; Bodnar, 1990). The intensity of fluorescence increases with the size of inclusions.

Quartz and calcite associated with the stibnite-bearing mineralization usually host primary inclusions that, at room temperature, have two phases (L + V) and a uniform degree of fill around 0.85 (Fig. 17D, E). The initial melting temperature between –50° and –56°C indicates presence of divalent cations (Fig. 18). Final melting of hydrohalite ($T_{m\ hyd1}$) was recorded between –27.2° and –39.0°C (Fig. 18). Ice melting temperatures ($T_{m\ ice}$) from –10.5° to –13.1°C (Fig. 18) suggest the salinity between 14.5 and 17.1 wt % NaCl equiv. Homogenization into liquid phase occurred from 120° to 165°C (Fig. 18).

Microthermometric measurements carried out on primary L + V inclusions hosted by realgar, orpiment, dolomite, and lorandite (Fig. 17F-I) have first melting temperatures (T_e) between –50° and –54°C, indicating the presence of divalent cations (Fig. 18). Melting runs between –35° and 0°C provide evidence for the existence of two hydrates. Melting of the first hydrate ($T_{m\ hyd1}$; sylvite) occurred between –22.0° and –24.5°C (Fig. 18). The final melting of the second hydrate ($T_{m\ hyd2}$; hydrohalite) was recorded between –11.0° and –15.4°C (Fig. 18). The final ice melting temperature ($T_{m\ ice}$) interval between –1.5° and –4.1°C (Fig. 18) corresponds to a salinity of 2.6 to 6.9 wt % NaCl equiv. The molar K/Na ratio calculated from hydrate melting temperatures varies between 0.19 and 0.21 (Hall et al., 1988). Homogenization of inclusions hosted by realgar and dolomite occurred into liquid

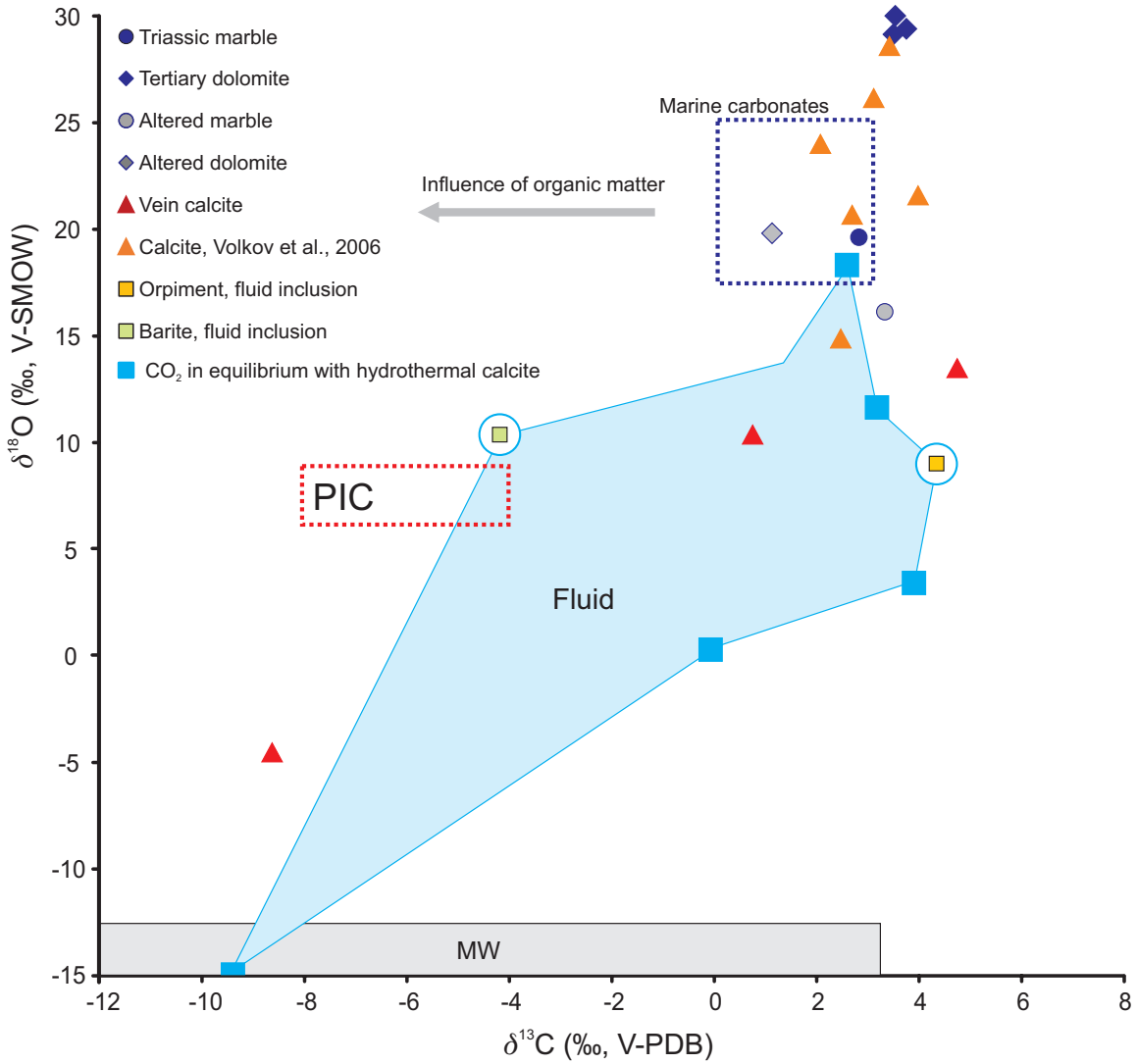

Fig. 15. Isotopic composition of carbonate host rocks, calcite, and fluid inclusion extracts from orpiment and barite relative to primary igneous carbonatite (PIC; Taylor et al., 1967), Phanerozoic marine carbonates (Veizer and Hoefs, 1976), and local meteoric water (MW). The blue fluid field shows the isotopic composition of water and CO_2 extracted from or in equilibrium with hydrothermal minerals. The results are indicative of carbonate rock buffered fluid, magmatic fluid, and variably exchanged meteoric water. Abbreviations: V-PBD = Vienna-Pee Dee belemnite, V-SMOW = Vienna-standard mean ocean water.

phase between 120° and 152°C (Fig. 18). Similar microthermometry data from realgar were published by Beran et al. (1990). The temperature of total homogenization within orpiment and lorandite was not recorded due to massive decrepitation of fluid inclusions at lower temperatures.

To identify major elements in hydrothermal fluids, scanning electron microscope-energy dispersive analyses of evaporate mounds produced by the thermal decrepitation of fluid inclusions were carried out according to the procedure described by Kontak (2004). Evaporate mounds that formed on the surfaces of quartz, realgar, and orpiment wafers were composed primarily of Cl, Na, and K. Traces of Ca were detected as well. Some inclusions hosted by realgar contain measurable amounts of Al and Si, probably indicating the presence of accidentally entrapped clay minerals.

Since no evidence of boiling was observed in the fluid inclusion assemblages studied, we infer that all were trapped in the one phase field along isochores that emanate from the solvus in the H_2O-NaCl-KCl-$CaCl_2$ ± CO_2 system. The wide range of T_h (102°–202°C) and salinities (2.6–21.3 wt % NaCl equiv) within and across the alteration zonation pattern is a clear evidence of mixing between saline and dilute liquids with different temperatures at the sites of ore deposition (Fig. 19). The occurrence of CO_2 in low- and high-temperature inclusions with different salinities probably reflects condensation of CO_2-rich vapor into aqueous liquids. The CO_2-rich vapor may have been produced by phase separation of ascending magmatic fluids and/or by dissolution of the carbonate host rocks by acid magmatic volatiles (e.g., HCl, SO_2 => H_2SO_4 + H_2S).

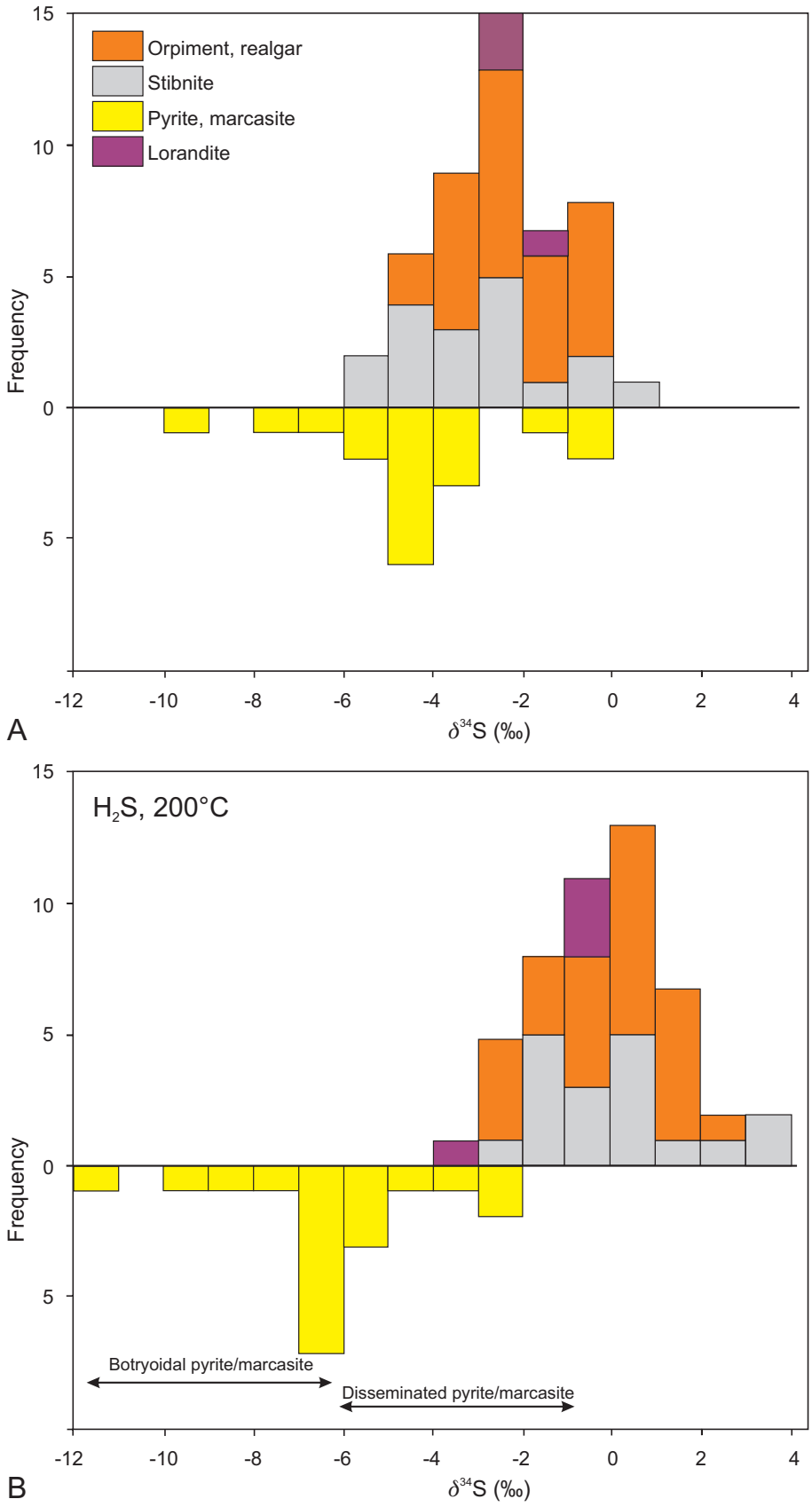

Fig. 16. (A) Sulfur isotope composition of Fe, Sb, and As sulfide minerals from the Allchar Au-As-Sb-Tl deposit. (B) Calculated composition of H_2S in equilibrium with the minerals at 200°C.

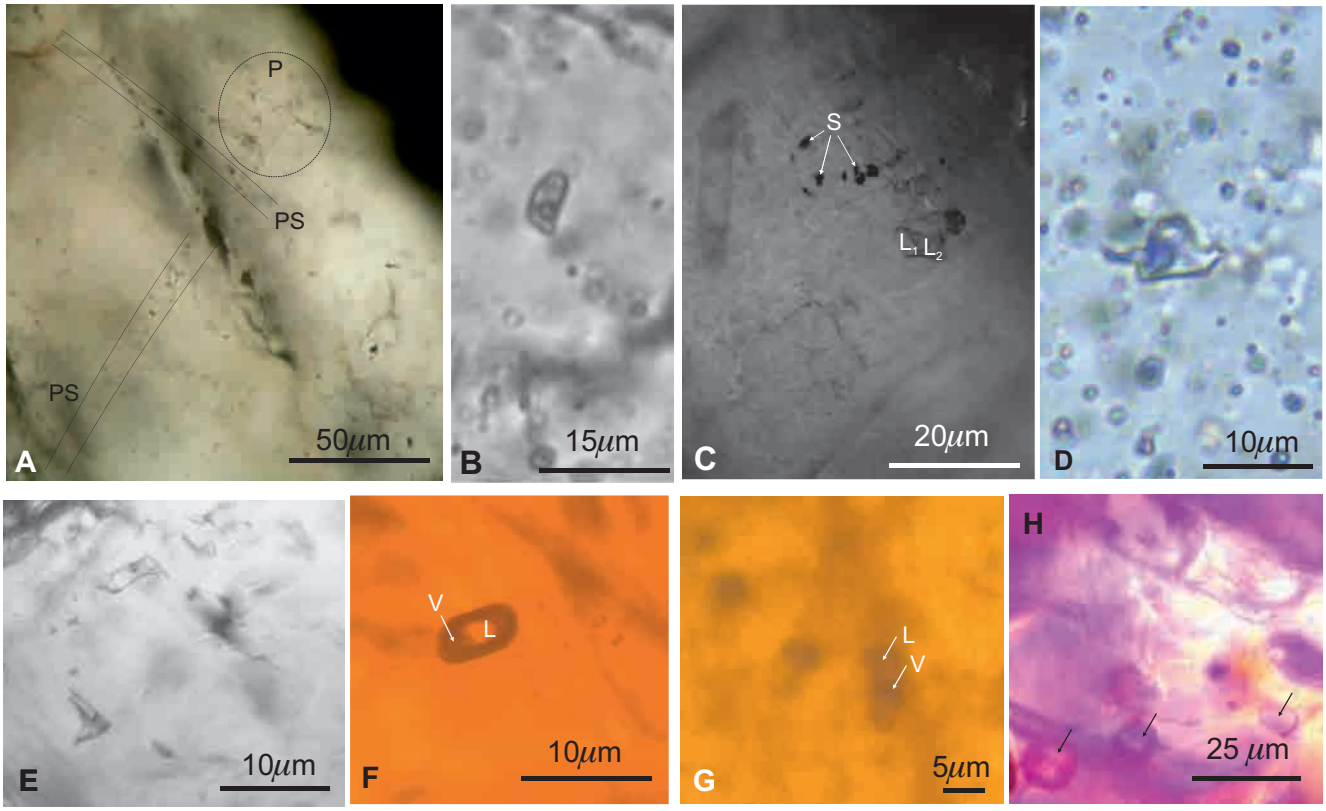

Fig. 17. Photomicrographs of fluid inclusions from the Allchar Au-As-Sb-Tl deposit. (A) Clusters of primary (P) and trails of pseudosecondary (PS) fluid inclusions hosted by quartz associated with the siliceous Au mineralization. (B) Primary aqueous-carbonic fluid inclusion hosted by stibnite-bearing jasperoid. (C) The hydrocarbon-bearing inclusions hosted by stibnite-bearing jasperoid contain one or more liquid (L_1, L_2) and/or solid (S) phases. (D) Primary aqueous fluid inclusion hosted by quartz associated with the stibnite-bearing mineralization. (E) Primary aqueous fluid inclusions hosted by calcite associated with the stibnite-bearing mineralization. (F) Primary aqueous fluid inclusion within realgar associated with the Tl-bearing mineralization. (G) Primary aqueous fluid inclusions hosted by orpiment associated with the Tl-bearing mineralization. (H) Primary aqueous fluid inclusions hosted by lorandite crystals. Abbreviations: L = liquid, V = vapor.

Chemical Reactions and Modeling

The isocon diagrams for the carbonate host rocks show that Au and Fe were introduced by hydrothermal solutions. Since Fe resides primarily in pyrite, S must also have been introduced (Fig. 10). As indicated by the absence of hypogene sulfate minerals, dissolution of calcite ± dolomite, and precipitation of marcasite and kaolinite, Eh-pH conditions favored $H_2S°$ over other S species. According to experimental data published by Stefansson and Seward (2004), in acid hydrothermal solutions with high a_{Cl^-}/a_{HS^-} ratios, Au chloride complexes predominate over Au bisulfide complexes. The following equation illustrates coprecipitation of Au and pyrite from a single fluid containing dissolved Au, Fe, and S:

$$AuCl_2^- + FeCl_2 + 2H_2S_{(aq)} \Leftrightarrow Au^0 + FeS_2 + 4H^+ + 4Cl^- \quad \Delta_rH << 0. \qquad (1)$$

At lower a_{Cl^-}/a_{HS^-} ratios the stability of Au bisulfide complexes is promoted, and Au and pyrite may precipitate by mixing between contrasting fluids, such as condensed magmatic vapor containing Au bisulfide complexes and saline liquids containing Fe chloride complexes:

$$Au(HS)_2^- + FeCl_2 \Leftrightarrow Au^0 + FeS_2 + 2H^+ + 2Cl^- \quad \Delta_rH << 0. \qquad (2)$$

In both cases, the neutralization of ore-forming fluids by the host carbonates will drive the reactions forward and promote deposition of Au and pyrite. These reactions would also be driven forward by an increase in pH produced by dilution with near-neutral groundwaters (Fig. 20).

In contrast, the isocon diagram for tuff shows that Fe was immobile (Fig. 10C), suggesting that sulfidation of preexisting Fe minerals, such as magnetite, in tuff was a critical factor for deposition of Au and pyrite:

$$3Au(HS)_2^- + Fe_3O_4 + 2H^+ \Leftrightarrow 3Au^0 + 3FeS_2 + 4H_2O \quad \Delta_rH << 0. \qquad (3)$$

Whereas all three reactions are exothermic over a wide range of pressures and temperatures, mixing of hot ore-bearing fluids with cold groundwaters will contribute to coprecipitation of Au and pyrite (Fig. 20).

In most hydrothermal solutions, As and Sb are transported by hydroxyl complexes (Pokrovski et al., 2002; Zotov et al., 2003; Seward et al., 2014), and their mobility depends on temperature, pressure, sulfur fugacity, redox potential, and pH value of the solution. The isocon diagrams indicate that deposition of As and Sb was accompanied by both silicification and argillic alteration. However, deposition of these minerals was more effective during low-temperature argillic alteration

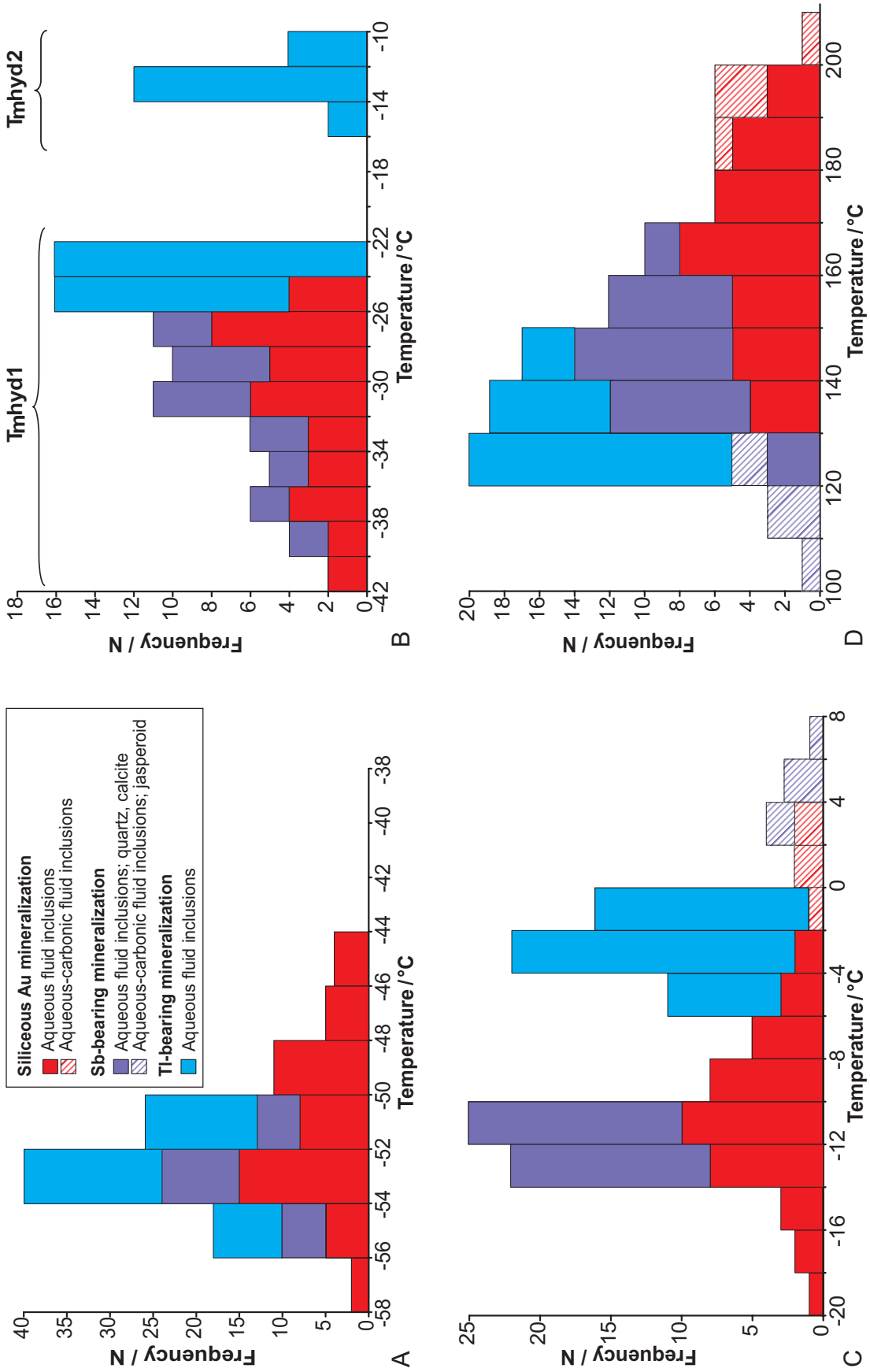

Fig. 18. Frequency distribution of (A) eutectic melting temperature, (B) final melting temperature of hydrates, (C) final melting temperature of ice, and (D) total homogenization temperature. The diagrams synthesize the new fluid inclusion data with the data previously published by Strmić Palinkaš et al. (2012).

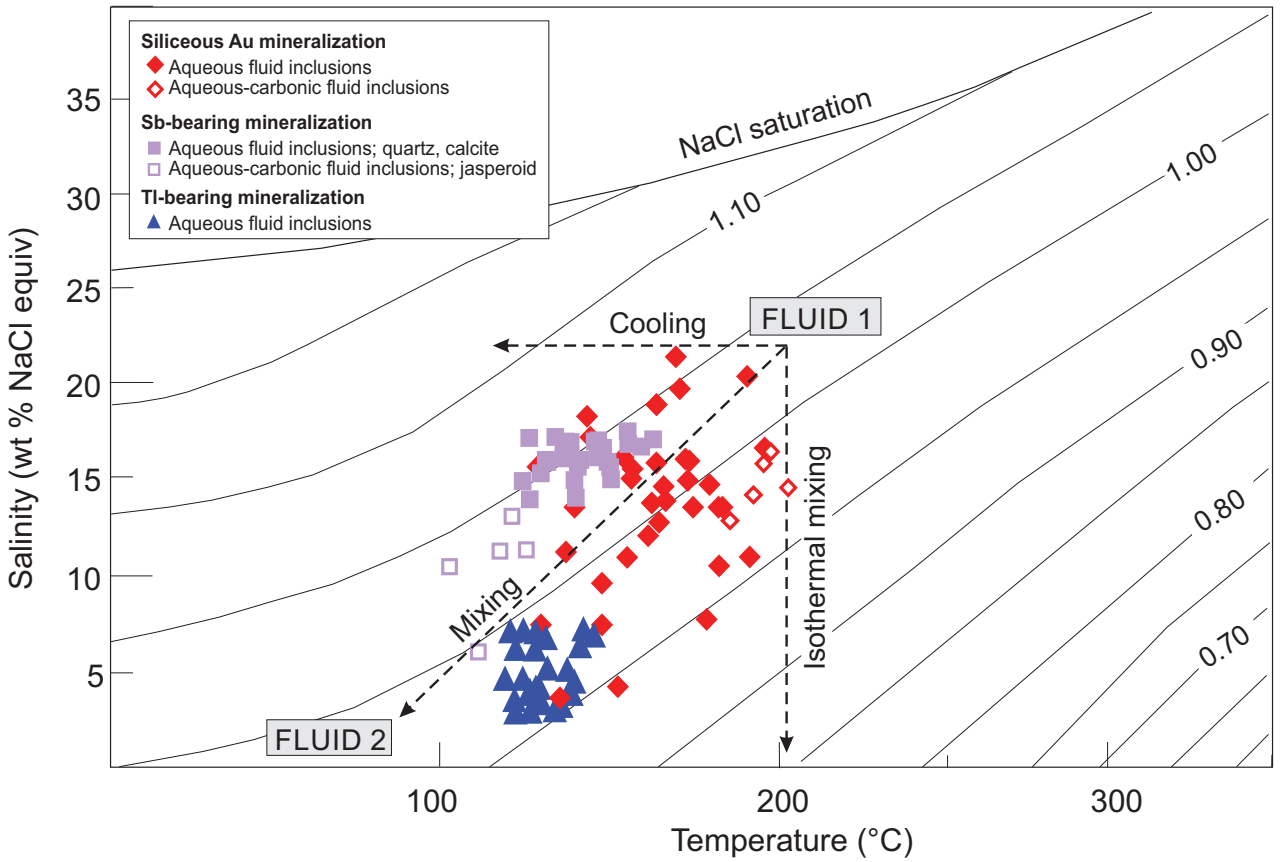

Fig. 19. Correlation of homogenization temperature and salinity for fluid inclusions hosted by the early siliceous Au mineralization, the main-stage Sb-bearing mineralization, and the late Tl-bearing mineralization.

(Fig. 10). Since stibnite, orpiment, and realgar have prograde solubility, this relationship suggests that cooling, acidification, and an increase in sulfur fugacity were key factors for precipitation of Sb and As sulfide minerals (Fig. 21):

$$As(OH)_{3(aq)} + H_2S_{(aq)} + H^+ \Leftrightarrow AsS + 3H_2O \quad \Delta_rH << 0 \quad (realgar) \qquad (4)$$

$$2As(OH)_{3(aq)} + 3H_2S_{(aq)} \Leftrightarrow As_2S_3 + 6H_2O \quad \Delta_rH << 0 \quad (orpiment) \qquad (5)$$

$$2Sb(OH)_{3(aq)} + 3H_2S_{(aq)} \Leftrightarrow Sb_2S_3 + 6H_2O \quad \Delta_rH << 0. \quad (stibnite) \qquad (6)$$

Although Au, Sb, and As occur together in hydrothermal solutions, differences in the stability of their complexes as hydrothermal conditions change affects their solubility ($Au_{solubility} << Sb_{solubility} < As_{solubility}$; Figs. 20, 21), which may account for the geochemical zonation observed at Allchar (Fig. 3).

Although the chemical properties of Tl are well known, its behavior in geologic processes is still vague. Thallium is an incompatible heavy metal that in aqueous solutions mostly exists in monovalent (thallous) oxidation state, although the trivalent (thallic) oxidation state is stable under extremely oxidizing conditions. Monovalent Tl^+ behaves like alkali metals (e.g., K^+), and it is mobile under acid to near-neutral hydrothermal conditions. In contrast, Tl^{3+} behaves similar to Al^{3+} and shows very limited mobility under hydrothermal conditions (e.g., Kemper and Bertram, 1991; Sobott, 1993). Monovalent Tl^+ prevails in reducing environments characterized by the predomination of sulfide over sulfate. Complexing of Tl^+ in hydrothermal solution greatly depends on temperature and pH conditions (Bebie et al., 1998; Xiong, 2007). According to thermodynamic data published by Xiong (2007) for 200°C, Tl^+ is the dominant species in acidic solutions, $TlHS^0$ is dominant in the neutral to moderate alkaline pH range, whereas $TlCO_3^-$ and $TlOH^0$ prevail in extremely alkaline solutions. Lorandite is the major solubility-controlling phase in As-bearing hydrothermal systems (Xiong, 2007).

The lack of Tl enrichment in the Au-rich part of the Allchar deposit suggests that sulfidation of Tl^+ at low pH and relatively high temperature was not an effective precipitation mechanism:

$$Tl^+ + Au(HS)_2^- + As(OH)_3 + H^+ \Leftrightarrow Au + TlAsS_2 + 3H_2O \quad (lorandite). \qquad (7)$$

The isocon diagrams show a tight link between Tl and the low-temperature argillic alteration as well as significant correlation between Tl and K (Fig. 10). Fluid inclusion data also suggest that the Tl-bearing mineralization was deposited from cooled and diluted fluids (Fig. 18) enriched in KCl. The Tl mineralization is spatially related to dolomite suggesting that,

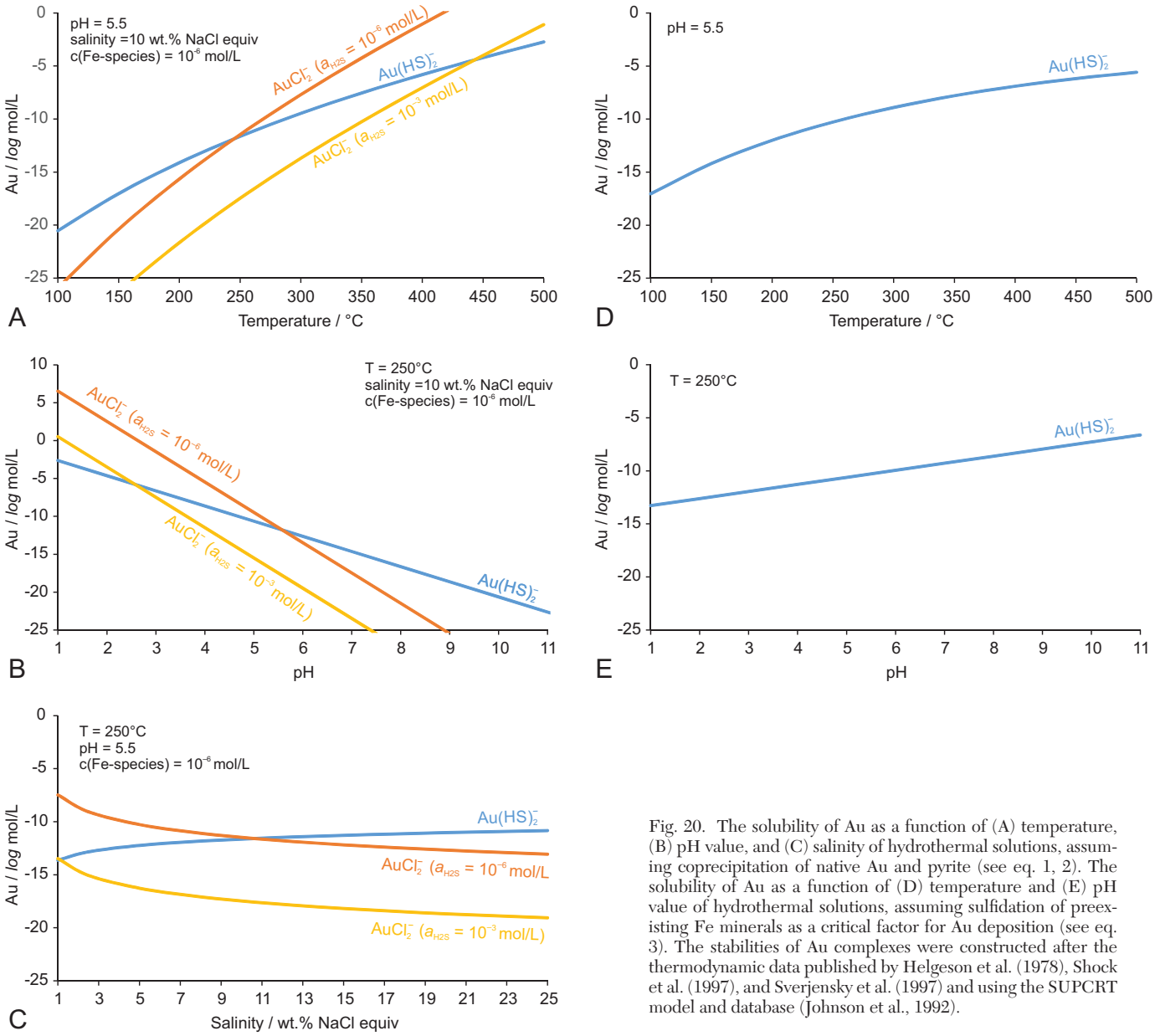

Fig. 20. The solubility of Au as a function of (A) temperature, (B) pH value, and (C) salinity of hydrothermal solutions, assuming coprecipitation of native Au and pyrite (see eq. 1, 2). The solubility of Au as a function of (D) temperature and (E) pH value of hydrothermal solutions, assuming sulfidation of preexisting Fe minerals as a critical factor for Au deposition (see eq. 3). The stabilities of Au complexes were constructed after the thermodynamic data published by Helgeson et al. (1978), Shock et al. (1997), and Sverjensky et al. (1997) and using the SUPCRT model and database (Johnson et al., 1992).

in addition to cooling, an increase in the pH of mineralizing fluids was critical to deposition of Tl:

$$Tl^{+} + As(OH)_3 + 2H_2S_{(aq)} \Leftrightarrow TlAsS_2 + 3H_2O + H^{+} \quad (8)$$

(*lorandite*).

This reaction is driven forward by neutralization of acid hydrothermal fluids by carbonate rocks and hydrolysis of framework silicates.

Discussion

Model for the formation of the Allchar Au-As-Sb-Tl deposit

After collision of the Adriatic and Euroasian plates along the Vardar zone, overprinting Cretaceous subduction-related magmatism, early Tertiary contraction, exhumation, and formation of an Eocene erosion surface, the Vardar zone tectonic mélange was the site of Oligocene to Pleistocene episodes of extensional faulting and calc-alkaline to shoshonitic magmatism that produced an assortment of Cu-Au porphyry, skarn, hydrothermal polymetallic (Pb-Zn ± Ag) replacement, and epithermal deposits. Field relationships and geochronology show that the Allchar Au-Sb-As-Tl deposit is spatially and temporally associated with a Pliocene (~5 Ma) shoshonitic volcano-plutonic center on the northern side of a NE-trending volcanic field with mineralization hosted in Pliocene tuff and subvolcanic intrusions, tuffaceous dolomite, and Triassic marble (Fig. 3). Stable isotopic, fluid inclusion, and trace element data suggest that concealed intrusions in this center were the source of metal- and ligand-bearing fluids and heat that drove circulation of meteoric ground water. Although isotopic data show that some lead and sulfur were leached from country rocks, the abundance

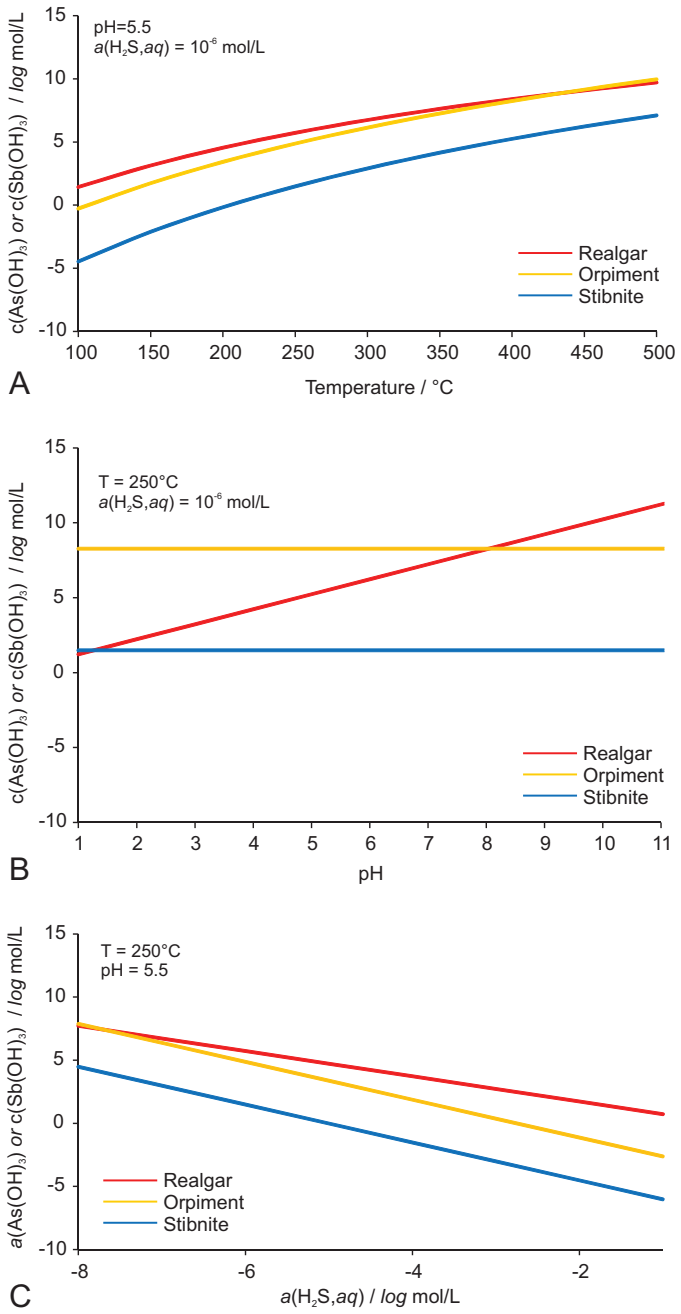

Fig. 21. The solubility of realgar (eq. 4), orpiment (eq. 5), and stibnite (eq. 6) as a function of (A) temperature, (B) pH value, and (C) activity of $H_2S_{(aq)}$ in hydrothermal solutions. The solubility curves were constructed after the thermodynamic data published by Helgeson et al. (1978), Pokrovski et al. (1996), Zotov et al. (2003), and Perfetti et al (2008) and using the SUPCRT model and database (Johnson et al., 1992).

of Cu, Sn, Te, and Se in stibnite, orpiment, realgar, and lorandite suggests that these metalloids were derived from magmas. The zonation from southern Au and Sb mineralization to northern As and Tl mineralization is perpendicular to the axis of the volcanic field and, together with variations in the fluid inclusion and isotopic data, suggests that fluid flow was from south to north. Mineralization appears to have occurred at the interface between ascending magmatic fluids and convecting groundwater on the northern side of the system. The localization of jasperoids and mineralization at structural intersections within fault breccias and fracture zones and along the Eocene unconformity shows that fluid flow was controlled by permeable structures and stratigraphy (Fig. 3B).

Fluid inclusion studies preclude boiling as a depositional mechanism but provide evidence that fluids with different salinities and temperatures mixed at the site of ore deposition. Isocon diagrams and chemical modeling suggest that decarbonatization, silicification, argillic alteration, and Au, Sb, As, and Tl mineralization formed in response to cooling and neutralization of acidic ore fluids by reactions with carbonate rocks and external ground water. Auriferous arsenian pyrite precipitated by cooling, mixing, and neutralization in carbonate host rocks and by sulfidation of Fe in tuff. Quartz and stibnite precipitated in response to cooling, realgar and orpiment by cooling and acidification, and lorandite by cooling and neutralization. The acidic character of the ore fluids was probably due to the condensation of magmatic vapor and dissociation of acid volatiles (CO_2, SO_2, HCl) into cool rocks and ground water. Quaternary faulting, uplift, and erosion exposed the deposits at the surface.

Comparison with Carlin-type gold deposits in Nevada

The Allchar deposit is similar to Nevada Carlin-type gold deposits in that it occurs near a terrain-bounding fault (Vardar zone) in an area of low-magnitude extension and intense magmatism. It is mostly hosted in subvolcanic calcareous and dolomitic sedimentary rocks, and mineralization occurs at intersections of high-angle faults and permeable stratigraphy (e.g., Eocene unconformity). It has similar alteration types (carbonate dissolution, silicification, argillization), ore minerals (auriferous arsenian pyrite and marcasite, stibnite, realgar, orpiment, lorandite), high Au/Ag ratios, and low base metal contents (e.g., Radtke, 1985; Hofstra and Cline, 2000; Muntean et al., 2011). It lacks fluid inclusion evidence of boiling, some of the ore pyrite precipitated by sulfidation of tuff, late-stage minerals precipitated primarily by cooling, and the late-stage minerals contain S and Pb derived from country rocks.

It differs in that it is an isolated Au prospect with a close spatial and temporal relationship to a shoshonitic volcano-plutonic center in a mineral belt dominated by intrusion-related Cu-Au porphyry, skarn, and hydrothermal polymetallic deposits. It is clearly zoned (proximal Au-Sb to distal As-Tl), has more dolomitization and sericitic alteration, has more introduced Fe, Mg, K, and Tl and less Au in ore pyrite, and contains more Cu, Sn, Te, and Se in stibnite, realgar, orpiment, and lorandite. It has lower-temperature and higher-salinity fluid inclusions and clear isotopic evidence for magmatic water, CO_2, and H_2S, and most of the ore pyrite in carbonate rocks precipitated by fluid mixing (e.g., Radtke et al., 1980; Holland et al., 1988; Groff, 1996; Hofstra, 1997; Hofstra and Rye, 1998; Cline and Hofstra, 2000; Emsbo et al., 2003; Lubben et al., 2012). These differences suggest that it is the very shallow and/or distal manifestation of a concealed porphyry system and is best classified as a distal disseminated gold deposit.

Conclusions

The evidence presented in this article confirm that Carlin-style gold deposits can form in the shallow/distal part of

intrusion-centered hydrothermal systems. Gold, Sb, As, and Tl were introduced by hot (>200°C), saline (up to ~ 21 wt % NaCl equiv), moderately acidic (pH <5) fluids that carried traces of magmatic H_2S and CO_2. The mineral and chemical zonation in the district is a result of different transport mechanisms of Au, Sb, As, and Tl under hydrothermal conditions and may indicate a potential for additional gold mineralization under cover at the southern end of the district. The evidence from Allchar also suggests that Tl mineralization may be present in the most distal neutralized portions of other intrusion-centered hydrothermal systems.

Acknowledgments

The manuscript was substantially improved by the comments of Panagiotis Voudouris and John Muntean. Also we would like to acknowledge John Muntean for all his support and patience in editing this manuscript.

REFERENCES

Bačeva, K., Stafilov, T., and Matevski, V., 2014, Bioaccumulation of heavy metals by endemic Viola species from the soil in the vicinity of the As-Sb-Tl mine Allchar, Republic of Macedonia: International Journal of Phytoremediation, v. 16, p. 347–365.

Balić Žunić, T., Moelo, Y., Lonćar, Z., and Micheelsen, H., 1994, Dorallcharite, $Tl_{0.8}K_{0.2}Fe_3(SO_4)(OH)_6$, a new member of the jarosite-alunite family: European Journal of Mineralogy, v. 6, p. 255–263.

Bebie, J., Seward, T.M., and Hovey, J.K., 1998, Spectrophotometric determination of the stability of thallium (I) chloride complexes in aqueous solution up to 200°C: Geochimica et Cosmochimica Acta, v. 62, p. 1643–1651.

Beran, A., Gotzinger, M., and Rieck, B., 1990, Fluid inclusions in realgar from Allchar: Symposium on Thallium Neutrino Detection, Dubrovnik, Yugoslavia, October 9–12, 1990, Proceedings, p. 42.

Bodnar, R.J., 1990, Petroleum migration in the Miocene Monterey Formation, California, USA: Constraints from fluid-inclusion studies: Mineralogical Magazine, v. 54, p. 295–304.

Boev, B., 1988, Petrological, geochemical, and volcanic features of volcanic rocks of the Kozuf Mountains: Unpublished Ph.D. thesis, Goce Delcev University, Stip, Republic of Macedonia, 195 p.

Boev, B., and Jelenković, R., 2012, Allchar deposit in Republic of Macedonia—petrology and age determination: Petrology—New Perspectives and Applications, v. 64, p. 132–168.

Booden, M.A., Smith, I.E., Black, P.M., and Mauk, J.L., 2011, Geochemistry of the early Miocene volcanic succession of Northland, New Zealand, and implications for the evolution of subduction in the southwest Pacific: Journal of Volcanology and Geothermal Research, v. 199, p. 25–37.

Borojević Šoštarić, S., Cvetković, V., Neubauer, F., Palinkaš, L.A., Bernroider, M., and Genser, J., 2012, Oligocene shoshonitic rocks of the Rogozna Mts. (Central Balkan Peninsula): Evidence of petrogenetic links to the formation of Pb-Zn-Ag ore deposits: Lithos, v. 148, p. 176–195.

Borojević Šoštarić, S., Palinkaš, L.A., Neubauer, F., Hurai, V., Cvetković, V., Roller-Lutz, Z., Mandić, M., and Genser, J., 2013, Silver-base metal epithermal vein and listwanite hosted deposit, Crnac, Rogozna Mts., Kosovo, part II: A link between magmatic rocks and epithermal mineralization: Ore Geology Reviews, v. 50, p. 98–117.

Borojević Šoštarić, S., Palinkaš, A.L., Neubauer, F., Cvetković, V., Bernroider, M., and Genser, J., 2014, The origin and age of the metamorphic sole from the Rogozna Mts., western Vardar belt: New evidence for the one-ocean model for the Balkan ophiolites: Lithos, v. 192, p. 39–55.

Boynton, W.V., 1984, Cosmochemistry of the rare earth elements: Meteorite studies, *in* Henderson, P., ed., Rare earth element geochemistry: Elsevier, p. 63–114.

Božović, M., Prelević, D., Romer, R.L., Barth, M., Van Den Bogaard, P., and Boev, B., 2013, The Demir Kapija ophiolite, Macedonia (FYROM): A snapshot of subduction initiation within a back arc: Journal of Petrology, v. 54, p. 1427–1453.

Castillo, P.R., Janney, P.E., and Solidum, R.U., 1999, Petrology and geochemistry of Camiguin Island, southern Philippines: Insights to the source of adakites and other lavas in a complex arc setting: Contributions to Mineralogy and Petrology, v. 134, p. 33–51.

Claypool, G.E., Holser, W.T., Kaplan, I.R., Sakai, H., and Zak, I., 1980, The age curves of sulfur and oxygen isotopes in marine sulfate and their mutual interpretation: Chemical Geology, v. 28, p. 199–260.

Cline, J.S., and Hofstra, A.H., 2000, Ore-fluid evolution at the Getchell Carlin-type gold deposit, Nevada, USA: European Journal of Mineralogy, v. 12, p. 195–212.

Cline, J.S., Stuart, F.M., Hofstra, A.H., Premo, W., Riciputi, L., Tosdal, R.M., and Tretbar, D.R., 2003, Multiple sources of ore-fluid components at the Getchell Carlin-type gold deposit, Nevada, USA, *in* Eliopoulos D., et al., eds., Mineral exploration and sustainable development, v. 2: Rotterdam, Millpress, p. 965–968.

Cline, J.S., Hofstra, A.H., Muntean, J.L., Tosdal, R.M., and Hickey, K.A., 2005, Carlin-type gold deposits in Nevada: Critical geologic characteristics and viable models: Economic Geology 100th Anniversary Volume, p. 451–484.

Cvetković, L., Boronikhin, V.A., Pavičević, M.K., Krajnović, D., Gržetić, I., Libowitzky, E., Giester, G., and Tillmanns, E., 1995, Jankovićite, $Tl_5Sb_9(As, Sb)_4S_{22}$, a new TI sulfosalt from Allchar, Macedonia: Mineralogy and Petrology, v. 53, p. 125–131.

Cvetković, V., Knežević, V., and Pécskay, Z., 2000, Tertiary igneous formations of the Dinarides, Vardar zone, and adjacent regions: From recognition to petrogenetic implications: Geology and metallogeny of the Dinarides and the Vardar zone: Academy of Sciences and Arts of the Republic of Srpska, Collections and Monographs, v. 1, p. 245–253.

Cvetković, V., Prelević, D., Downes, H., Jovanović, M., Vaselli, O., and Pecskay, Z., 2004, Origin and geodynamic significance of Tertiary postcollisional basaltic magmatism in Serbia (central Balkan Peninsula): Lithos, v. 73, p. 161–186.

Dilek, Y., Furnes, H., and Shallo, M., 2007, Suprasubduction zone ophiolite formation along the periphery of Mesozoic Gondwana: Gondwana Research, v. 11, p. 453–475.

Dimitrijević, M.D., 2001, The Dinarides and the Vardar zone: A short review of the geology: Acta Vulcanologica, v. 13, p. 1–8.

Dumurdžanov, N., Serafimovski, T., and Burchfiel, B.C., 2004, Evolution of the Neogene-Pleistocene basins of Macedonia: Geological Society of America Digital Map and Chart Series, v. 1, p. 1–20.

Emsbo, P., Hofstra, A.H., Lauha, E.A., Griffin, G.L., and Hutchinson, R.W., 2003, Origin of high-grade gold ore, source of ore fluid components, and genesis of the Meikle and neighboring Carlin-type deposits, northern Carlin trend, Nevada: Economic Geology, v. 98, p. 1069–1105.

Erkul, F., and Erkul, T.S., 2010, Geology of the early Miocene Alaçamdağ (Dursunbey-Balikesir) magmatic complex and implications for the western Anatolian extensional tectonics: Mineral Research and Exploration, v. 141, p. 1–25.

Frantz, E., Palme, H., Todt, W., Goresy, A.E., and Pavičević, M., 1994, Geochemistry of Tl-As minerals and host rocks at Allchar (FYR Macedonia): Neues Jahrbuch fur Mineralogie-Abhandlungen, v. 167, p. 359–400.

Friedman, I., and O'Neil, J.R., 1977, Compilation of stable isotope fractionation factors of geochemical interest: U.S. Geological Survey Professional Paper 440–KK, 12 p.

Gao, J., John, T., Klemd, R., and Xiong, X., 2007, Mobilization of Ti-Nb-Ta during subduction: evidence from rutile-bearing dehydration segregations and veins hosted in eclogite, Tianshan, NW China: Geochimica et Cosmochimica Acta, v. 71, p. 4974–4996.

Giesemann, A., Jager, H.-J., Norman, A.L., Krouse, H.R., and Brand, W.A., 1994, Online sulfur-isotope determination using an elemental analyzer coupled to a mass spectrometer: Analytical Chemistry, v. 66, p. 2816–2819.

Grant, J.A., 2005, Isocon analysis: A brief review of the method and applications: Physics and Chemistry of the Earth, Parts A/B/C, v. 30, p. 997–1004.

Groff, J.A., 1996, $^{40}Ar/^{39}Ar$ geochronology of gold mineralization and origin of auriferous fluids for the Getchell and Twin Creeks mines, Humbolt County, Nevada: Unpublished Ph.D. dissertation, Socorro, New Mexico, New Mexico Institute of Mining and Technology, 291 p.

Hagemann, H.W., and Hollerbach, A., 1986, The fluorescence behaviour of crude oils with respect to their thermal maturation and degradation: Organic Geochemistry, v. 10, p. 473–480.

Hall, D.L., Sterner, S.M., and Bodnar, R.J., 1988, Freezing point depression of NaCl-KCl-H_2O solutions: Economic Geology, v. 83, p. 197–202.

Hastie, A.R., Kerr, A.C., Pearce, J.A., and Mitchell, S.F., 2007, Classification of altered volcanic island arc rocks using immobile trace elements: Development of the Th-Co discrimination diagram: Journal of Petrology, v. 48, p. 2341–2357.

Helgeson, H.C., Delany, J.M., Nesbitt, H.W., and Bird, D.K., 1978, Summary and critique of the thermodynamic properties of rock-forming minerals: American Journal of Science, v. 278A, p. 1–229.

Hofstra, A.H., 1997, Isotopic composition of sulfur in Carlin-type Au deposits: Implications for genetic models: Economic Geology Guidebook Series, v. 28, p. 119–131.

Hofstra, A.H., and Cline, J.S., 2000, Characteristics and models for Carlin-type gold deposits: Reviews in Economic Geology, v. 13, p. 163–220.

Hofstra, A.H., and Rye, R.O., 1998, δD and δ^{18}O data from Carlin-type gold deposits: Implications for genetic models: U.S. Geological Survey Open-File Report 98-338, p. 202–210.

Holland, P.T., Beaty, D.W., and Snow, G.G., 1988, Comparative elemental and oxygen isotope geochemistry of jasperoid in the northern Great Basin; evidence for distinctive fluid evolution in gold-producing hydrothermal systems: Economic Geology, v. 83, p. 1401–1423.

Ilić Jr., M., 1988, Genetic types of magnesite deposits in freshwater Miocene basins of Yugoslavia (in Serbian): Vesnik Zavoda za Geoloska i Gefizicka Istrazivanja, v. 28, p. 25–57.

Ivanov, T., 1965, Zonal distribution of elements and minerals in the deposit Alsar: Symposium on Problems of Postmagmatic Ore Deposition II, Geological Society of Czechoslovakia, Prague, Czech Republic, September 10–27, 1963, Proceedings, p. 186–191.

——1986, Allchar, the richest ore deposit of Tl in the world: Workshop on the Feasibility of Solar Neutrino Detection with ^{205}Pb by Geochemical and Accelerator Mass Spectroscopical Measurements, Darmstadt, Germany, April 1986, Proceedings, GSI-report 86-9.

Jakupi, B., Kostić, A., Antanasijević, R., Jovanović, L., Todorović, Z., Perelygin, V.P., and Stetsenko, S.G., 1982, Određivanje geološke starosti auripigmenta iz Alšara (Makedonija) metodom tragova fisionih fragmenata(in Serbian): Glasnik Prirodnjackog Muzeja u Beogradu. Serija A: Mineralogija, geologija, paleontologija, v. 37, p. 135–143.

Janković, S., 1979, Antimony deposits of southeastern Europe: Savezni Zavod za Geološka i geofizička istraživanja, v. 37, p. 25–48.

——1993, Metallogenic features of the Alshar epithermal Sb-As-Tl deposit (the Serbo-Macedonian metallogenic province): Neues Jahrbuch fur Mineralogie-Abhandlungen, v. 166, p. 25–41.

——1995, The principal metallogenic features of the Kopaonik district: Geology and metallogeny of the Kopaonik Mountains Symposium, Belgrade, Serbia, June 19–22, 1995, p. 79–101.

——1997, The Carpatho-Balkanides and adjacent area: A sector of the Tethyan Eurasian metallogenic belt: Mineralium Deposita, v. 32, p. 426–433.

Janković, S., and Jelenković, R., 1994, Thallium mineralization in the Allchar Sb-As-Tl-Au deposit: Neues Jahrbuch fur Mineralogie-Abhandlungen, v. 167, p. 283–298.

Janković, S., Boev, B., and Serafimovski, T., 1997, Magmatism and Tertiary mineralization of the Kozuf metallogenetic district, Republic of Macedonia, with particular reference to the Allchar deposit: University of Belgrade Faculty of Mining and Geology, Special Publication, v. 5, 262 p.

Johnson, J.W., Oelkers, E.H., and Helgeson, H.C., 1992, SUPCRT92: A software package for calculating the standard molal thermodynamic properties of minerals, gases, aqueous species, and reactions from 1 to 5,000 bar and 0° to 1,000°C: Computers and Geosciences, v. 18, p. 899–947.

Jolivet, L., and Brun, J.-P., 2010, Cenozoic geodynamic evolution of the Aegean region: International Journal of Earth Sciences, v. 99, p. 109–138.

Jurković, I., Palinkaš, L.A., Garašić, V., and Strmić Palinkaš, S., 2012, Genesis of vein-stockwork cryptocrystalline magnesite from the Dinaride ophiolites: Ofioliti, v. 37, p. 13–26.

Karamata, S., 2006, The geological development of the Balkan Peninsula related to the approach, collision, and compression of Gondwanan and Eurasian units: Geological Society, London, Special Publications, v. 260, p. 155–178.

Karamata, S., Majer, V., and Pamić, J., 1980, Ophiolites of Yugoslavia: Ofioliti: v. 1, p. 105–125.

Karamata, S., Knežević, V., Pecskay, Z., and Djordjević, M., 1997, Magmatism and metallogeny of the Ridanj-Krepoljin belt (eastern Serbia) and their correlation with northern and eastern analogues: Mineralium Deposita, v. 32, p. 452–458.

Karamata, S., Olujić, J., Protić, Lj., Milovanović, D., Vujnović, L., Popević, A., Memović, E., Radovanović, Z., and Resimić-Šarić, K., 2000, The western belt of the Vardar zone—the remnant of a marginal sea, *in* Karamata, S., and Janković, S., eds., Geology and metallogeny of the Dinarides and the Vardar zone: Zvornik, Academy of Science and Arts of Republika Srpska, p. 131–135.

Kemper, F.H., and Bertram, H.P., 1991, Thallium, *in* Merian, E., and Clarkson, T.W., eds., Metals and their compounds in the environment: Occurrence, analysis, and biological relevance, v. 29, Weinheim, Germany, VCH Verlagsgesellschaft MBH, p. 1227–1241.

Kesler, S.E., Russell, N., Seaward, M., Rivera, J., McCurdy, K., Cumming, G.L., and Sutter, J.F., 1981, Geology and geochemistry of sulfide mineralization underlying the Pueblo Viejo gold-silver oxide deposit, Dominican Republic: Economic Geology, v. 76, p. 1096–1117.

Kolios, N., Innocenti, F., Manetti, P., Peccerillo, A., and Giuliani, O., 1980, The Pliocene volcanism of the Voras Mountains (Central Macedonia, Greece): Bulletin Volcanologique, v. 43, p. 553–568.

Kontak, D.J., 2004, Analysis of evaporate mounds as a complement to fluid-inclusion thermometric data: Case studies from granitic environments in Nova Scotia and Peru: Canadian Mineralogist, v. 42, p. 1315–1329.

Koroneos, A., Poli, G., Cvetković, V., Christofides, G., Krstic, D., and Pécskay, Z., 2011, Petrogenetic and tectonic inferences from the study of the Mount Cer pluton (West Serbia): Geological Magazine, v. 148, p. 89–111.

Large, R.R., Bull, S.W., and Maslennikov, V.V., 2011, A carbonaceous sedimentary source-rock model for Carlin-type and orogenic gold deposits: Economic Geology, v. 106, p. 331–358.

Le Bas, M.J., Le Maitre, R.W., Streckeisen, A., and Zanettin, B., 1986, A chemical classification of volcanic rocks based on the total alkali-silica diagram: Journal of Petrology, v. 27, p. 745–750.

Lehmann, St., Barcikowski, J., von Quadt, A., Gallhofer, D., Peytcheva, I., Heinrich, C.A., and Serafimovski, T., 2013, Geochronology, geochemistry, and isotope tracing of the Oligocene magmatism of the Buchim-Damjan-Borov Dol ore district: Implications for timing, duration, and source of the magmatism: Lithos, v. 180, p. 216–233.

Lippolt, H.J., and Fuhrmann, U., 1986, K-Ar age determination on volcanics of Alshar mine/Yugoslavia: Workshop on the Feasibility of Solar Neutrino Detection with ^{206}Pb by Geochemical and Mass Spectroscopical Measurements, Darmstadt, Germany, April 1986, Proceedings, Report GSI-86-9.

Lubben, J.D., Cline, J.S., and Barker, S.L., 2012, Ore fluid properties and sources from quartz-associated gold at the Betze-Post Carlin-type gold deposit, Nevada, United States: Economic Geology, v. 107, p. 1351–1385.

Martin, H., 1999, Adakitic magmas: Modern analogues of Archaean granitoids: Lithos, v. 46, p. 411–429.

McCrea, J.M., 1950, On the isotope chemistry of carbonates and a paleotemperature scale: Journal of Chemical Physics, v. 18, p. 849–857.

McDonough, W.F., and Sun, S.S., 1995, The composition of the Earth: Chemical Geology, v. 120, p. 223–253.

McLimans, R.K., 1987, The application of fluid inclusions to migration of oil and diagenesis in petroleum reservoirs: Applied Geochemistry, v. 2, p. 585–603.

Melfos, V., and Voudouris, P., 2017, Cenozoic metallogeny of Greece and potential for precious, critical, and rare metals exploration: Ore Geology Reviews, v. 89, p. 1030–1057.

Mercier, J.L., 1973, Etude géologique des zones internes des Hellénides en Macédoine centrale (Grèce).(I re thèse). Contribution à l'étude de l'évolution magmatique et du métamorphisme des zones internes des Hellénes: Annales Géologique des Pays Helléniques, v. 20, 792 p.

Muntean, J.L., Cline, J.S., Simon, A.C., and Longo, A.A., 2011, Magmatic-hydrothermal origin of Nevada's Carlin-type gold deposits: Nature Geoscience, v. 4, p. 122–127.

Neubauer, F., Pavicevic, M.K., Genser, J., Jelenković, R., Boev, B., and Amthauer G., 2009, ^{40}Ar/^{39}Ar dating of geological events of the Allchar deposit and its host rocks: Geochimica et Cosmochimica Acta, v. 73, Supplement 1, A938.

Ohmoto, H., 1972, Systematics of sulfur and carbon isotopes in hydrothermal ore deposits: Economic Geology, v. 67, p. 551–578.

Ohmoto, H., and Rye, R.O., 1979, Isotopes of sulfur and carbon, *in* Barnes, H.L., ed., Geochemistry of hydrothermal ore deposits, 2nd ed.: New York, Wiley, p. 509–567.

Ozen, Y., and Arik, F., 2015, S, O, and Pb isotopic evidence on the origin of the Inkaya (Simav-Kütahya) Cu-Pb-Zn-(Ag) prospect, NW Turkey: Ore Geology Reviews, v. 70, p. 262–280.

Pavičević, M.K., and El Goresy, A., 1988, Crven Dol Tl deposit in Allchar: Mineralogical investigation, chemical composition of Tl minerals, and genetic implications: Nuclear instruments and methods in physics research section A: Accelerators, spectrometers, detectors and associated equipment, v. 271, p. 297–300.

Peccerillo, A., and Taylor, S.R., 1976, Geochemistry of Eocene calc-alkaline volcanic rocks from the Kastamonu area, northern Turkey: Contributions to Mineralogy and Petrology, v. 58, p. 63–81.

Percival, T.J., and Radtke, A.S., 1993a, Gold mineralization of the Carlin-type in the Alšar district, SR Macedonia, Yugoslavia, *in* Maurice, Y.T., ed.: Proceedings of the eighth quadrennial IAGOD symposium, Ottawa, Canada, Stuttgart, E. Schweizerbart'sche Verlagsbuchhandlung, p. 637–646.

——1993b, Thallium in disseminated replacement gold deposits of the Carlin-type; a preliminary report: Neues Jahrbuch fur Mineralogie Abhandlungen, v. 166, p. 65–75.

——1994, Sedimentary-rock-hosted disseminated gold mineralization in the Alsar district, Macedonia: Canadian Mineralogist, v. 32, p. 649–665.

Perfetti, E., Pokrovski, G.S., Ballerat-Busserolles, K., Majer, V., and Gibert, F., 2008, Densities and heat capacities of $As(OH)_3^0{}_{(aq)}$, $AsO(OH)_3^0{}_{(aq)}$, and iron sulfarsenide minerals: Geochimica et Cosmochimica Acta, v. 72, p. 713–731.

Pokrovski, G.S., Gout, R., Schott, J., Zotov, A., and Harrichoury, J.C., 1996, Thermodynamic properties and stoichiometry of As (III) hydroxide complexes at hydrothermal conditions: Geochimica et Cosmochimica Acta, v. 60, p. 737–749.

Pokrovski, G.S., Zakirov, I.V., Roux, J., Testemale, D., Hazemann, J., Bychkov, A.Y., and Golikova, G.V., 2002, Experimental study of arsenic speciation in vapor phase to 500°C: Implications for As transport and fractionation in low-density crustal fluids and volcanic gases: Geochimica et Cosmochimica Acta, v. 66, p. 3453–3480.

Prelević, D., Foley, S.F., Romer, R.L., Cvetković, V., and Downes, H., 2005, Tertiary ultrapotassic volcanism in Serbia: Constraints on petrogenesis and mantle source characteristics: Journal of Petrology, v. 46, p. 1443-1487.

Radtke, A.S., 1985, Geology of the Carlin gold deposit, Nevada: U.S. Geological Survey Professional Paper 1267, 221 p.

Radtke, A.S., Rye, R.O., and Dickson, F.W., 1980, Geology and stable isotope studies of the Carlin gold deposit, Nevada: Economic Geology, v. 75, p. 641–672.

Rakičević, T., and Pendzerkovski, J., 1970, Explanatory notes for the general geological map of Kožuf (1:100,000): Federal Geological Survey, Beograd, p. 1–47.

Reich, M., Kesler, S.E., Utsunomiya, S., Palenik, C.S., Chryssoulis, S.L., and Ewing, R.C., 2005, Solubility of gold in arsenian pyrite: Geochimica et Cosmochimica Acta, v. 69, p. 2781–2796.

Ridley, W.I., and Lichte, F.E., 1998, Major, trace, and ultratrace element analysis by laser ablation ICP-MS: Reviews in Economic Geology, v. 7, p. 199–215.

Robertson, A.H., Trivić, B., Đerić, N., and Bučur, I.I., 2013, Tectonic development of the Vardar ocean and its margins: Evidence from the Republic of Macedonia and Greek Macedonia: Tectonophysics, v. 595, p. 25–54.

Roedder, E., 1984, Fluid inclusions: Reviews in Mineralogy, v. 12, 644 p.

Rumsey, M.S., Mills, S.J., Spratt, J., Hay, D.G., and Farber, G., 2014, Thalliumpharmacosiderite, IMA 2013-124: Mineralogical Magazine, v. 78, p. 549–558.

Schefer, S., Cvetković, V., Fügenschuh, B., Kounov, A., Ovtcharova, M., Schaltegger, U., and Schmid, S.M., 2011, Cenozoic granitoids in the Dinarides of southern Serbia: Age of intrusion, isotope geochemistry, exhumation history, and significance for the geodynamic evolution of the Balkan Peninsula: International Journal of Earth Sciences, v. 100, p. 1181–1206.

Seward, T.M., Williams-Jones, A.E., and Migdisov, A.A., 2014, The chemistry of metal transport and deposition by ore-forming hydrothermal fluids: Treatise on Geochemistry, 2nd ed., v. 13, p. 29–57.

Sharp, I.R., and Robertson, A.H., 2006, Tectonic-sedimentary evolution of the western margin of the Mesozoic Vardar ocean: Evidence from the Pelagonian and Almopias zones, northern Greece: Geological Society, London, Special Publications, v. 260, p. 373–412.

Shock, E.L., Sassani, D.C., Willis, M., and Sverjensky, D.A., 1997, Inorganic species in geologic fluids: Correlations among standard molal thermodynamic properties of aqueous ions and hydroxide complexes: Geochimica et Cosmochimica Acta, v. 61, p. 907–950.

Sobott, R.J.G., 1993, Environmental aspects of thallium: Neues Jahrbuch fur Mineralogie-Abhandlungen, v. 166, p. 77–81.

Stefansson, A., and Seward, T.M., 2004, Gold(I) complexing in aqueous sulphide solutions to 500°C at 500 bar: Geochimica et Cosmochimica Acta, v. 68, p. 4121–4143.

Stolz, A.J., Jochum, K.P., Spettel, B., and Hofmann, A.W., 1996, Fluid- and melt-related enrichment in the subarc mantle: Evidence from Nb/Ta variations in island-arc basalts: Geology, v. 24, p. 587–590.

Strmić Palinkaš, S., Borojević Šoštarić, S., Palinkaš, L., Pecskay, Z., Boev, B., and Bermanec, V., 2012, Fluid inclusions and K/Ar dating of the Allšar Au-Sb-As-Tl mineral deposit, Macedonia: Geologica Macedonica, v. 24, p. 63–71.

Strmić Palinkaš, S., Palinkaš, L.A., Renac, C., Spangenberg, J.E., Lüders, V., Molnar, F., and Maliqi, G., 2013, Metallogenic model of the Trepča Pb-Zn-Ag skarn deposit, Kosovo: Evidence from fluid inclusions, rare earth elements, and stable isotope data: Economic Geology, v. 108, p. 135–162.

Strmić Palinkaš, S., Palinkaš, L.A., Mandić, M., Roller-Lutz, Z., Pécskay, Z., Maliqi, G., and Bermanec, V., 2016, Origin and K/Ar age of the phreatomagmatic breccia at the Trepča Pb-Zn-Ag skarn deposit, Kosovo: Implications for ore-forming processes: Geologia Croatica, v. 69, p. 121–142.

Sudar, M., and Kovacs, S., 2006, Metamorphosed and ductilely deformed conodonts from Triassic limestones situated beneath ophiolite complexes: Kopaonik Mountain (Serbia) and Bükk Mountains (NE Hungary)—a preliminary comparison: Geologica Carpathica, v. 57, p. 157–176.

Sverjensky, D.A., Shock, E.L., and Helgeson, H.C., 1997, Prediction of the thermodynamic properties of aqueous metal complexes to 1,000°C and 5 kb: Geochimica et Cosmochimica Acta, v. 61, p. 1359–1412.

Taylor, H.P., Frechen, J., and Degens, E.T., 1967, Oxygen and carbon isotope studies of carbonatites from the Laacher See district, West Germany and the Alnö district, Sweden: Geochimica et Cosmochimica Acta, v. 31, p. 407–430.

Troesch, M., and Frantz, E., 1992, $^{40}Ar/^{39}Ar$ Alter der Tl-As mine von Crven Dol, Allchar, Macedonia (in German): Berichte der Deutschen Mineralogischen Gesellschaft, v. 4, p. 276.

von Quadt, A., Moritz, R., Peytcheva, I., and Heinrich, C.A., 2005, Geochronology and geodynamics of Late Cretaceous magmatism and Cu-Au mineralization in the Panagyurishte region of the Apuseni-Banat-Timok-Srednogorie belt (Bulgaria): Ore Geology Reviews, v. 27, p. 95–126.

Vasković, N., and Matović, V., 2010, Ophiolites of the Vardar zone and the Dinarides: Central and West Serbia: Acta Mineralogica-Petroghraphica, Field Guide Series, v. 24, p. 1–55.

Veizer, J., and Hoefs, J., 1976, The nature of O^{18}/O^{16} and C^{13}/C^{12} secular trends in sedimentary carbonate rocks: Geochimica et Cosmochimica Acta, v. 40, p. 1387–1395.

Veselinović-Williams, M., 2011, Characteristics and origin of polymetallic mineralisation in the Kopaonik region of Serbia and Kosovo, with particular reference to the Belo Brdo Pb-Zn (Ag) deposit: Unpublished Ph.D. thesis, London, Kingston University, 150 p.

Volkov, A.V., Serafimovski, T., Kochneva, N.T., Tomson, I.N., and Tasev, G., 2006, The Alshar epithermal Au-As-Sb-Tl deposit, southern Macedonia: Geology of Ore Deposits, v. 48, p. 175–192.

Xiong, Y., 2007, Hydrothermal thallium mineralization up to 300°C: A thermodynamic approach: Ore Geology Reviews, v. 32, p. 291–313.

Yanev, Y., Boev, B., Doglioni, C., Innocenti, F., Manetti, P., Pecskay, Z., Tonarini, S., and D'Orazio, M., 2008, Late Miocene to Pleistocene potassic volcanism in the Republic of Macedonia: Mineralogy and Petrology, v. 94, p. 45–60.

Zartman, R.E., and Doe, B.R., 1981, Plumbotectonics—the model: Tectonophysics, v. 75, p. 135–162.

Zelić, M., Agostini, S., Marroni, M., Pandolfi, L., and Tonarini, S., 2010, Geological and geochemical features of the Kopaonik intrusive complex (Vardar zone, Serbia): Ofioliti, v. 35, p. 33–47.

Zimmerman, A., Stein, H.J., Hannah, J.L., Koželj, D., Bogdanov, K., and Berza, T., 2008, Tectonic configuration of the Apuseni-Banat-Timok-Srednogorie belt, Balkans-South Carpathians, constrained by high precision Re-Os molybdenite ages: Mineralium Deposita, v. 43, p. 1–21.

Zotov, A.V., Shikina, N.D., and Akinfiev, N.N., 2003, Thermodynamic properties of the Sb(III) hydroxide complex $Sb(OH)_{3(aq)}$ at hydrothermal conditions: Geochimica et Cosmochimica Acta, v. 67, p. 1821–1836.